

On the dependence of simulated convection on domain size

Andrea M Jenney¹ and Zeyuan Hu²

¹Oregon State University

²Harvard University

February 16, 2024

Abstract

We present a heuristic model to quantitatively explain the suppression of deep convection in convection-resolving models (CRMs) with small domains. We distinguish between “computational” smallness (few grid columns) and “physical” smallness (representing a small geographic area). Domains that are computationally small require greater instability to sustain convection because they force a large convective fraction, driving strong compensating subsidence warming. Consequently, detrainment occurs lower for undiluted convection. Both computationally and physically small domains limit the physical updraft width, increasing entrainment dilution. This enhancement of entrainment strengthens the sensitivity to domain size beyond that for undiluted deep convection. Coarsening grid spacing to expand the physical domain and physical updraft width can reduce domain size sensitivity. Simulations using the System for Atmospheric Modeling (SAM) confirm the heuristic model results. We also present simulation results for two shallow convection cases, which are less sensitive to domain size, but also exhibit sensitivities.

On the dependence of simulated convection on domain size

A. M. Jenney¹, Z. Hu²

¹College of Earth, Ocean, and Atmospheric Sciences, Oregon State University

²Department of Earth and Planetary Sciences, Harvard University

Key Points:

- Deep convection is suppressed in domains with few grid columns due to strong subsidence warming and entrainment into small updrafts
- This effect can be reduced by increasing grid spacing
- Small domains are more humid than large domains regardless of grid spacing because of enhanced convective mixing

Corresponding author: Zeyuan Hu, zeyuan.hu@fas.harvard.edu

Corresponding author: Andrea Jenney, andrea.jenney@oregonstate.edu

12 **Abstract**

13 We present a heuristic model to quantitatively explain the suppression of deep con-
 14 vection in convection-resolving models (CRMs) with small domains. We distinguish be-
 15 tween “computational” smallness (few grid columns) and “physical” smallness (repre-
 16 senting a small geographic area). Domains that are computationally small require greater
 17 instability to sustain convection because they force a large convective fraction, driving
 18 strong compensating subsidence warming. Consequently, detrainment occurs lower for
 19 undiluted convection. Both computationally and physically small domains limit the phys-
 20 ical updraft width, increasing entrainment dilution. This enhancement of entrainment
 21 strengthens the sensitivity to domain size beyond that for undiluted deep convection.
 22 Coarsening grid spacing to expand the physical domain and physical updraft width can
 23 reduce domain size sensitivity. Simulations using the System for Atmospheric Model-
 24 ing (SAM) confirm the heuristic model results. We also present simulation results for
 25 two shallow convection cases, which are less sensitive to domain size, but also exhibit sen-
 26 sitivities.

27 **Plain Language Summary**

28 We present a simple mathematical model that helps explain why cloudy upward
 29 air movement (convection) is suppressed in “small” computer simulations used for study-
 30 ing weather. We look at two types of “smallness”: one is about the computer’s limita-
 31 tions (fewer grid columns), and the other is about how big the area that is being rep-
 32 resented would be on a map (physical size). When the computer model has fewer columns,
 33 more energy is needed for upward air movement because the compressive warming of sink-
 34 ing air around clouds is stronger. This affects where air stops moving upward (detrain-
 35 ment).

36 Both types of smallness make the upward air column narrower in a physical sense,
 37 causing more outside air to mix in (entrainment). Because cloudy air is typically warmer
 38 and more humid than the air around it, this mixing reduces the temperature of the cloudy
 39 air and weakens the upward air movement. We found that increasing the number of columns
 40 or making the columns wider can help reduce these effects. We tested this in simulations
 41 and our results support our simple mathematical model.

42 **1 Introduction**

43 Convection-resolving models (CRMs) are popular tools used to simulate large-scale
 44 turbulent motions associated with clouds and convection. In stand-alone simulations, CRMs
 45 are oftentimes run with domains as small as 100 km to inhibit the spontaneous cluster-
 46 ing of the convective region in a phenomenon known as convective self aggregation (e.g.,
 47 Wing et al., 2018, 2020), which occurs preferentially in larger domains (Muller & Held,
 48 2012; Yanase et al., 2020). In addition, small CRM domains are often used in general
 49 circulation models (GCMs) employing superparameterization (SP), also known as multi-
 50 scale modeling framework (MMF), in which the convective parameterization is replaced
 51 with many embedded CRMs. Recent SP/MMF simulations use CRMs with as few as
 52 64 columns to reduce computational cost (e.g., Hannah et al., 2020, 2022; Lin et al., 2022).

53 Many studies exploring the sensitivity of standalone CRM simulations to domain
 54 size focus on convective self aggregation (Muller & Held, 2012; Patrizio & Randall, 2019;
 55 Yanase et al., 2020). These studies have shown that convective self-aggregation tends
 56 to occur at domain sizes larger than 200 km. In CRM simulations forced with observa-
 57 tions M. F. Khairoutdinov and Randall (2001) find that the precipitable water increased
 58 and rainfall fraction decreased with increasing domain size. However, these simulations

59 varied in dimensionality, horizontal resolution, and vertical resolution, so inferring the
60 isolated impacts of varying domain size is not possible.

61 Sensitivity to CRM domain size has also been studied in modern SP setups. Liu
62 et al. (2023) compare 2-D simulations of the Energy Exascale Earth System Model-MMF
63 (E3SM-MMF) with 32 total columns to 3-D simulations with 32 grid columns in each
64 horizontal dimension (1024 total columns) and find large differences in mean precipita-
65 tion and its statistics over some tropical regions. Whether the differences were driven
66 entirely by differences in domain size in the CRMs or by their dimensionality is unclear.
67 Peng et al. (2022) find differences in cloud fractions up to 0.4 and absorbed shortwave
68 radiation up to 60 W m^{-2} in some regions when comparing E3SM-MMF simulations with
69 32 vs. 64 CRM columns. E3SM-MMF with 2D CRMs with high horizontal resolution
70 (200 m) but small domains (12.8 km) appeared to under-resolve larger eddies important
71 for marine boundary layer clouds (Peng et al., 2023). As in other studies, the different
72 horizontal resolutions associated with different CRM domain sizes of Peng et al. (2022)
73 and Peng et al. (2023) makes disentangling the effects of domain size from horizontal res-
74 olution a challenge.

75 Few studies have explicitly studied the isolated impact of CRM domain size inde-
76 pendent of horizontal resolution on convective behavior and the mean atmospheric state
77 for the small domain sizes used in SP models. Pritchard et al. (2014) found that decreas-
78 ing the CRM domain size from 32 to 8 columns (while keeping horizontal resolution con-
79 stant) led to an increase in the climate sensitivity of an SP GCM, primarily due to changes
80 in low-level cloudiness. They propose a convective “throttling” hypothesis grounded in
81 buoyancy, in which small CRM domains limit the frequency that deep convection can
82 occur because of strong warming by compensating subsidence occurring over a fraction-
83 ally smaller area than is possible in a large CRM domain. This occurs because the min-
84 imum updraft size is limited by the fraction of the domain occupied by a single grid col-
85 umn, which increases as the number of grid columns decreases. As a result of convec-
86 tive throttling, the lower troposphere remains less ventilated in small CRM domains, re-
87 sulting in increased lower tropospheric humidity, denser liquid clouds, and a cooler up-
88 per troposphere. Despite these differences, the mean tropical radiative cooling rate is in-
89 sensitive to domain size, which implies a broader distribution of simulated deep convec-
90 tion at the smallest CRM scales due to infrequent yet intense deep convection needed
91 to balance the radiative cooling. These ideas can be traced back to Bjerknes (1938), who
92 provided a similar argument to explain the observed smallness of the tropical updraft
93 fraction.

94 Despite these advances, a *quantitative* understanding of the mechanisms of the rela-
95 tionship between domain size and mean atmospheric properties remains limited. For
96 example, the domain size at which convergence occurs and how domain size sensitivi-
97 ties interact with horizontal resolution sensitivities (e.g., Jeevanjee & Zhou, 2022) both
98 remain unclear. Motivated by the fact that small domain CRM simulations continue to
99 be run both as standalone simulations and in SP GCMs, this study aims to quantita-
100 tively explore the mechanisms proposed in Pritchard et al. (2014) using CRM experi-
101 ments (i.e., without the host GCM) with relatively “small” domain sizes (i.e., domain
102 sizes smaller than required for convective self-aggregation).

103 2 Methods

104 2.1 Experimental Setup

105 We use the System for Atmosphere Modeling (SAM; Khairoutdinov and Randall
106 2003), version 6.10.6, configured as a cloud-resolving model. A simple Smagorinsky-type
107 scheme (M. F. Khairoutdinov & Randall, 2003) computes sub-grid scale momentum and
108 scalar tendencies. We run both deep and shallow convective cases.

109 All deep convective simulations use 60 vertical levels with a model top located near
 110 26km and a rigid-lid top boundary condition. The vertical grid spacing linearly increases
 111 from 75m near the surface up to 2.5km, above which it is held constant at 500m. A sponge
 112 layer is located above 18km. The radiation scheme is the Rapid and Accurate Radia-
 113 tive Transfer Model for General Circulation Models (RRTMG) (Iacono et al. 2008). We
 114 use a constant solar insolation (no diurnal cycle) with fixed solar constant of 683.5 W
 115 m⁻² and zenith angle of 50.5°. Domain-averaged horizontal wind is nudged to zero at each
 116 vertical level with a nudging time scale of 1 hr. Sea surface temperature is fixed uniformly
 117 at 303K. Deep convective simulations are initialized from predefined initial temperature
 118 and moisture profiles and spun up for 100 days. White noise temperature perturbations
 119 on the order of 0.01K are applied to the lowest 5 model layers to initialize convection.
 120 Unless otherwise noted, a 20-day period after spin-up is used to compute equilibrium statis-
 121 tics. Domain-mean statistics are sampled every 2 min and then averaged to estimate hourly
 122 domain-mean statistics. Instantaneous 3-D fields are saved every 30 minutes.

123 We present results from 3-D deep convective simulations with 1 km horizontal resolu-
 124 tion and 8, 16, 32, 64, 128, 256 grid cells in each horizontal direction (“nx”). To ex-
 125 plore interactions between domain size and horizontal resolution sensitivity, we further
 126 ran 3 additional sets of simulations with 4km, 250m, and 62.5m resolution. For complete-
 127 ness, we also ran two-dimensional simulations with 16 and 128 columns, which we omit
 128 results from because of their close similarity to the 3-D runs.

129 For shallow convective simulations, We used large scale forcings, boundary condi-
 130 tions, and initial profiles from two field studies: the Barbados Oceanographic and Me-
 131 teorological EXperiment (BOMEX) (Holland & Rasmusson, 1973) as in Siebesma et al.
 132 (2003) to simulate shallow cumulus (“trade” cumulus) and the first research flight of the
 133 second Dynamics and Chemistry of Marine Stratocumulus (DYCOMS-RF01) (Stevens
 134 et al., 2005) to simulate marine stratocumulus. For these shallow convection simulations,
 135 we used a fixed horizontal resolution of 125 m and a fixed vertical resolution of 25 m with
 136 128 vertical levels. The DYCOMS-RF01 simulations are initialized with the same white
 137 noise temperature perturbation method as the deep convective simulations. The BOMEX
 138 simulations were initialized with white noise temperature perturbations on the order of
 139 0.1 K and water vapor perturbations on the order of 0.025 g kg⁻¹ applied to the low-
 140 est 1.6 km. Shallow convection simulations were run for 6 hours with a time step of 2
 141 seconds. Unlike the deep convective simulations, here we turned off precipitation. We
 142 do not include radiation in the BOMEX simulation, and use a simple interactive long-
 143 wave radiation calculation as in Stevens et al. (2005) for DYCOMS-RF01. We present
 144 results with 8, 16, 32, 64, 128 grid cells in each horizontal direction. Domain-mean statis-
 145 tics are sampled every 20 seconds and then averaged to estimate minute-mean domain-
 146 mean statistics.

147 We ran ensembles of the shallow convective cases to enhance the signal to noise ra-
 148 tio. These ensembles were initialized using different random numbers for the initial white
 149 noise perturbation. Most simulations have 64 ensemble members. However, for specific
 150 cases, we adjusted the number of members: we present 1024 members for the nx=8 BOMEX
 151 case, and 256 members for the nx=16 BOMEX and the nx=16 DYCOMS-RF01 cases.

152 **2.2 Methods for diagnosing entrainment and detrainment rate**

153 In later sections, we will present some results relating to diagnosed fractional en-
 154 trianment and detrainment rate. Here we document how they are calculated. We first
 155 estimate the entrainment and detrainment rate through a simple entraining-detraining
 156 bulk-plume model:

$$157 \quad \frac{\partial \phi_u}{\partial z} = -\epsilon(\phi_u - \phi_n) + S_u \quad (1)$$

$$158 \quad \frac{1}{M} \frac{\partial M}{\partial z} = \epsilon - \delta \quad (2)$$

159

160 where ϕ is a relatively conserved variable, subscripts “u” and “n” denote averages across
 161 convective updraft grid cells and non-updraft grid cells, S_u is the net source of ϕ within
 162 updraft, ϵ and δ represent the fractional entrainment rate and detrainment rates, and
 163 M represents the convective updraft mass flux. Here, we define ϕ_u as the water vapor
 164 plus cloud water mixing ratio. S_u is evaporation of precipitation minus cloud-to-precipitation
 165 conversion averaged across updraft grid cells, and is zero for our shallow convection sim-
 166 ulations where we turned off precipitation. Convective updraft grid cells are those with
 167 cloud mixing ratios greater than 10^{-5} kg kg $^{-1}$ and upward vertical velocities greater than
 168 1 m s $^{-1}$. Non-updraft grid cells are defined as those with cloud water mixing ratios smaller
 169 than 10^{-5} kg kg $^{-1}$. Horizontally averaged ϕ_u , ϕ_n , S_u , and M were saved as part of our
 170 domain-mean statistics outputs.

171 In addition to the above single plume model, we also used a spectrum plume method
 172 to diagnose entrainment rate distribution (Kuang & Bretherton, 2006). Unlike the sin-
 173 gle plume model which assumes all the updrafts have the same entrainment rate profile,
 174 the spectrum plume model allows updrafts to have a spectrum of entrainment rates. Here
 175 we briefly describe the procedure of calculating entrainment rate distribution used in (Kuang
 176 & Bretherton, 2006). First we need to calculate the convective updraft mass flux dis-
 177 tribution in the space of frozen moist static energy (FMSE) and height. FMSE is defined
 178 as $c_p T + gz + L_v q - L_f q_i$. Then we can specify a set of fractional entrainment rate val-
 179 ues, and calculating the FMSE profile of an entraining plume using the mean FMSE in
 180 the updraft at the cloud base for each fractional entrainment rate. Then, at each level,
 181 we can count how many mass flux falls into each entrainment rate interval according to
 182 their FMSE. Essentially we get mass flux distribution in the space of entrainment rate
 183 and height.

184 3 Domain “smallness” and its impacts

185 Domain size has a clear impact on mean state quantities of limited-domain CRM
 186 simulations. For deep convective simulations, Figure 1a-c shows mean profiles of con-
 187 vective mass flux, cloud fraction, and relative humidity, each of which decrease through-
 188 out the troposphere with increasing domain size. Larger domains are also colder below
 189 10 km, and warmer above (Figure 1d).

190 A CRM domain may be small in two ways: it may be computationally small by
 191 having few grid columns, and it also may be physically small by covering a small phys-
 192 ical area. Increasing the horizontal grid spacing increases the physical domain size of a
 193 computationally fixed domain size (i.e., fixed number of grid columns). In the discus-
 194 sion that follows, we will present a heuristic argument to explain how computational small-
 195 ness leads to convective throttling and how this may be partially compensated by increas-
 196 ing the physical domain size.

197 The net circulation over a limited domain is the sum of the convective and envi-
 198 ronmental mass fluxes,

$$199 \quad \bar{w} = w_c \sigma_c + w_e \sigma_e, \quad (3)$$

200 where w is vertical velocity, σ is the fractional area of convection (subscript c) and en-
 201 vironment (subscript e), and the over bar indicates a domain mean quantity. In writ-
 202 ing (3), we have ignored any horizontal variation in density. In both SP-CESM and E3SM-
 203 MMF, $\bar{w} = 0$ throughout the CRM domain. We thus omit \bar{w} from subsequent equa-
 204 tions.

205 If environmental air is sinking ($w_e < 0$), it warms due to adiabatic compression
 206 at the rate given by $w_e(\Gamma_e - \Gamma_d)$, where $\Gamma = -\partial T/\partial z$ is the lapse rate and Γ_d is the
 207 dry adiabatic lapse rate. Using Equation (3) and the fact that the fractional areas of con-

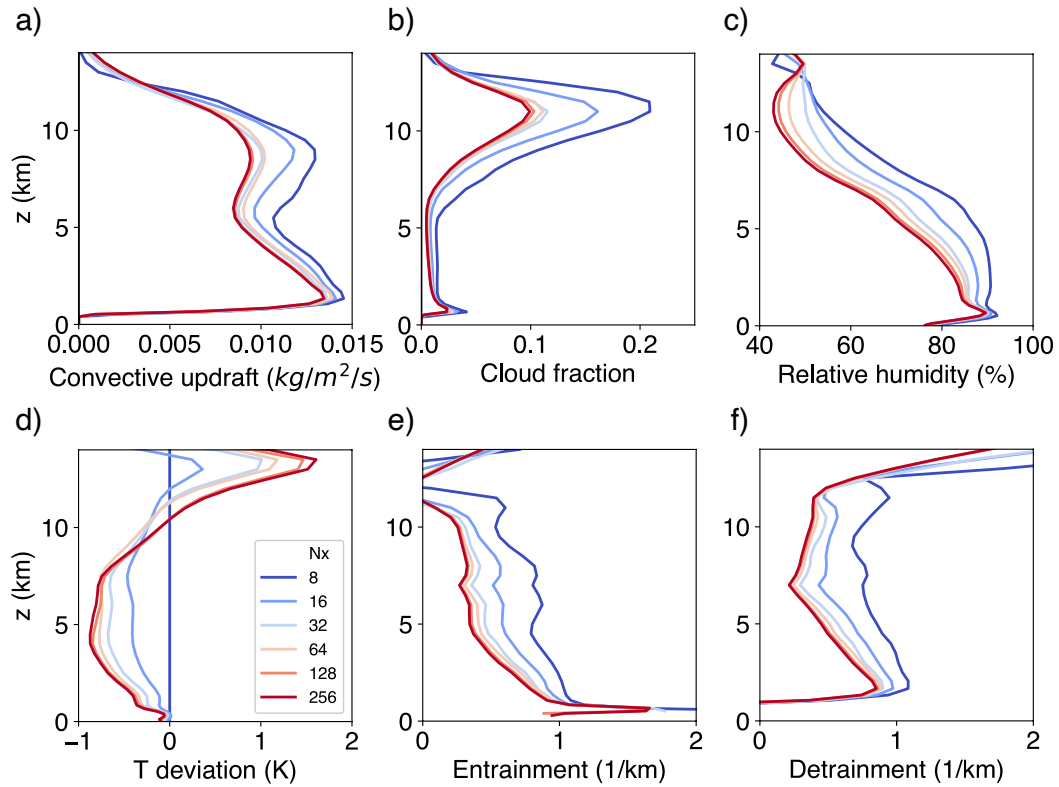


Figure 1. Dependence of atmospheric profiles on domain size for deep convective simulations: (a) updraft mass flux, (b) cloud fraction, (c) relative humidity, (d) temperature deviation from $n_x=8$, (e) fractional entrainment rate and (f) fractional detrainment rate. Entrainment and detrainment are diagnosed using the bulk plume model described in Section 2.2.

vection and of the environment must sum to one, we can write subsidence warming in the descent region as

$$\frac{dT_e}{dt} = -\frac{w_c \sigma_c}{1 - \sigma_c} (\Gamma_e - \Gamma_d). \quad (4)$$

The rate that temperature changes in the ascent region during undilute moist convection is

$$\frac{dT_c}{dt} = w_c (\Gamma_c - \Gamma_m), \quad (5)$$

where Γ_m is the saturated adiabatic lapse rate. To sustain a buoyancy-driven convective overturning circulation, positive buoyancy of the convective region is required. This means that the convective region must maintain a positive virtual temperature difference from the surrounding, descending environment. We can approximate this condition as

$$\frac{dT_c}{dt} > \frac{dT_e}{dt}, \quad (6)$$

which we can re-write in terms of the ascent area using Eqs. (4) and (5) as,

$$\sigma_c < \frac{\Gamma_c - \Gamma_m}{\Gamma_d - \Gamma_m + \Gamma_c - \Gamma_e}. \quad (7)$$

Equation (7) describes a limit on the maximum possible fractional convective area in a limited-domain CRM with no mean circulation by the lapse rates of the convective and non-convective region. The largest σ_c that can exist during ongoing convection increases with the instability of the convective region (Γ_c). Conversely, convective area is limited when instability is small. This is a consequence of condition (6). Because subsidence warming is stronger for faster sinking motion, small ascent areas ensure that subsidence warming is weak by being spread over a large area (Bjerknes, 1938). Second, in addition to the instability of the convective region, Equation (7) also shows that horizontal temperature gradients exert a limit on σ_c . When $\Gamma_c - \Gamma_e$ is large, environmental air is more likely to be warmer than convective region air. Thus, convective area must be small for large $\Gamma_c - \Gamma_e$ to keep w_e small and maintain positive convective region buoyancy. In CRM domains using superparameterized models, this effect may be second-order due to the relative smallness of CRM domains and the resulting closeness of Γ_c and Γ_e . For $\Gamma_c \approx \Gamma_e = \bar{\Gamma}$, Equation (7) simplifies to

$$\sigma_c < \frac{\bar{\Gamma} - \Gamma_m}{\Gamma_d - \Gamma_m}. \quad (8)$$

3.1 Small computational domains require more instability to sustain convection

We thus arrive at the first way that small computational CRM domains “throttle” convection. Computational domain size limits the minimum value that σ_c can assume: The smallest possible value of σ_c in a CRM domain is $1/N$ where N is the number of grid columns. This number decreases as the computational domain size and the number of grid columns increases.

For $\Gamma_c \approx \Gamma_e$ (a close approximation in a small domain), the threshold instability (Γ^*) at which a sustained convectively-driven overturning circulation is supported given a minimum possible σ_c (σ_c^*) can be inferred from Equation (8) as:

$$\Gamma^* > \sigma_c^* (\Gamma_d - \Gamma_m) + \Gamma_m \quad (9)$$

Equation (9) shows that as the computational domain size increases and σ_c^* decreases, Γ^* also decreases. As σ_c^* approaches zero, Γ^* approaches Γ_m . Figure 2 shows Γ^* computed from Equation (9) for domains with computational sizes ranging from 2 columns to 512 columns. For undilute convection (solid lines), this critical instability converges for domains larger than about 32 columns (a common number for SP simulations).

Buoyant convection doesn't occur without entrainment. Equation (5) can be modified for entraining convection as

$$\frac{dT_c}{dt} = w_c(\Gamma_c - \Gamma_m - \epsilon\beta) \quad (10)$$

where ϵ is the fractional entrainment rate and β is a dilution factor that depends on the difference in temperature and humidity between the updraft air and the entrained air, which we will crudely approximate as

$$\beta = T_c - T_e + \frac{L_v}{c_p}(q_s - q_e). \quad (11)$$

In Equation (11), L_v is the latent heat of vaporization, c_p is the specific heat capacity of dry air, and q is the water vapor mixing ratio. In writing (11), we have assumed that the entrained air has the temperature and humidity of the environment and that the convective region is saturated (q_s). We have also neglected differences in latent heating due to ice processes.

When the effects of entrainment are considered in the dependence of Γ^* on domain size, convergence at large domain sizes diminishes. We illustrate this with an example in Figure 2, which shows Γ^* profiles computed using a modification of Equation (9) that includes entrainment with (10) and (11). We neglect temperature differences between the convective and non-convective region ($T_c - T_e = 0$). We apply a 1% decrease in the relative humidity for successive domain sizes (as in Figure 1c), and entrainment rates which decrease by 5% as the number of columns is doubled (as in Figure 1e; see Section 3.2). Figure 2 shows that incorporating the impact of entrainment on Γ^* reduces large domain size convergence. This is a consequence of the sensitivity of the entrainment rate to domain size (which we discuss in the next section), despite a contribution in the opposite direction by the spread in relative humidity with domain size.

In summary, one way small computational domains “throttle” convection is by requiring more instability to sustain convection due to large σ_c . As we will show in the next section, entrainment rates also decrease as domain size decreases. As a result, while there is convergent behavior in Γ^* for domains larger than 32 columns for undilute convection, differences in entrainment reduce this convergence, and differences in Γ^* with domain size exist even for computationally large domains.

3.2 Small domains limit updraft width and enhance convective mixing

The critical instability in Equation (9) is the threshold lapse rate for *one grid column* to buoyantly convect without violating condition (6). For a given value of $\Gamma > \Gamma^*$, the number of grid columns available for convection increases with the computational domain size. This implies, for a fixed grid size, that increasing the total number of columns also allows updrafts to be *physically* wider. Convective entrainment rates are larger for physically small updrafts (Morrison, 2017; Morrison et al., 2020). Thus, the second way that CRM domain size “throttles” convection is by limiting updraft width and reducing updraft buoyancy by enhancing dilution by entrainment.

Our simulations are consistent with this behavior. Figure 1e shows that the mean fractional entrainment rate decreases with increasing computational domain size (for a fixed grid spacing). This occurs because updrafts are forced to be physically small in small domains. Figure 3 shows distributions of entrainment rate and updraft width at 8 km

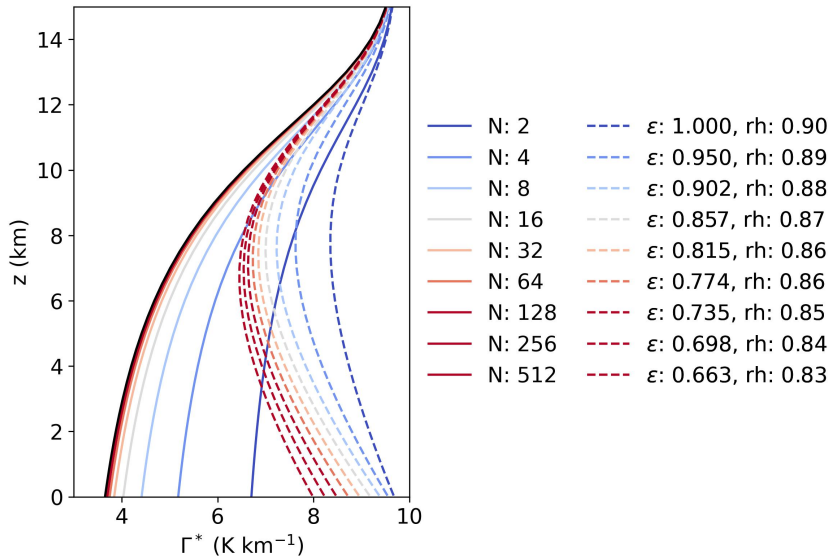


Figure 2. The critical lapse rate, Γ^* , needed to sustain a convective overturning circulation from Equation (9) for domains of different computational sizes. Here, “N” refers to the total number of grid columns. Solid lines show Γ^* for undilute convection. Dashed lines show Γ^* when idealized entrainment dilution is considered. Entrainment rates and relative humidities, which vary with the number of columns, (km^{-1}) are shown in the legend. Black line is the moist adiabatic lapse rate for a surface temperature of 300 K.

295 for square domains with 16, 64, and 256 columns in each horizontal dimension. As
 296 expected, updrafts are narrower in the small domain and entrainment rates are larger.
 297 The other two domain sizes are more similar, yet exhibit differences in line with our ex-
 298 pectations: the largest domain has slightly larger updrafts and slightly weaker entrain-
 299 ment rates.

300 For a small domain (such that $\sigma_c \approx \sigma_c^*$) at a computationally fixed size, increas-
 301 ing the grid spacing will make updrafts physically wider. Thus, we expect that they should
 302 also entrain less (Morrison, 2017; Morrison et al., 2020). Additional simulations with vary-
 303 ing horizontal resolution corroborate this expectation. Figure 4m-p shows entrainment
 304 rates for simulations with a range of computational domain sizes as grid spacing is de-
 305 creased from 4 km (left) to 62.5 m (right). As the grid spacing decreases and updrafts
 306 become smaller, the distribution of entrainment rates shifts towards larger values. Dif-
 307 ferences in the entrainment rate between resolutions are largest for the smallest domain.

308 In summary, computationally small domains increase convective entrainment rates
 309 because they limit updraft width. This impact can be reduced either by increasing the
 310 physical or computation domain size.

311 3.3 Convection in small domains detrains lower

312 Computationally small domains limit the minimum possible value that σ_c can as-
 313 sume. As a result of σ_c that is forced to be large, updrafts are inhibited by too-strong
 314 compensating subsidence (Section 3.1). In Section 3.2, we discussed how domain size lim-
 315 its updraft width, and enhances entrainment. It can be intuited that detrainment should
 316 also occur lower in small domains as a result of these combined effects. This is confirmed
 317 in our simulations. Figures 1f and 4q-t show that detrainment in simulated convection

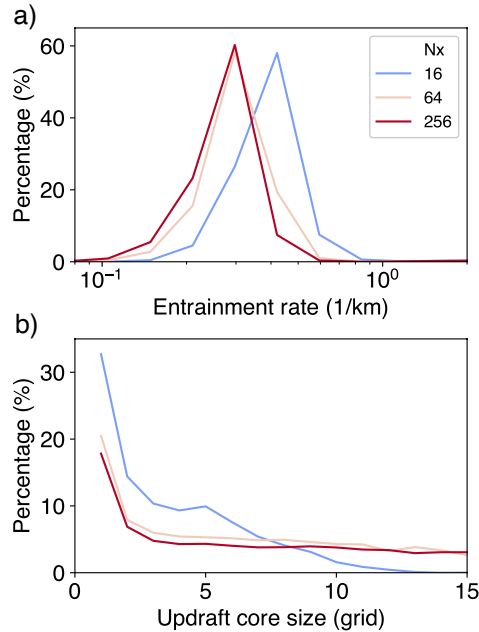


Figure 3. Probability distributions of (a) entrainment rate and (b) updraft width at 8 km. The entrainment rate distribution is diagnosed using the spectrum plume model described in Section 2.2. The core size distribution is calculated as the mass-flux-weighted number of updraft grid cells in each contiguous updraft core. A single core is determined as adjacent grid cells with upward velocity greater than 1 m s^{-1} and cloud mixing ratio greater than $10^{-5} \text{ kg kg}^{-1}$.

318 increases as computational domain sizes decreases. This is expected behavior even for
319 undilute convection.

320 Entrainment enhances this behavior. Updraft buoyancy reduction due to dilution
321 by entrainment is more likely as domain size decreases and updrafts become smaller. In
322 this way, enhanced entrainment also increases the impact of domain size on detrainment.
323 Figure 4q-t shows that as grid spacing decreases (and differences in entrainment between
324 computational domain sizes increases), the spread in detrainment rate with domain size
325 also increases, with the smallest domains at this highest resolution detraining the most.

326 **3.4 Domain size impacts on mean state variables and precipitation vari-** 327 **ability**

328 The mean relative humidity decreases with increasing computational and physi-
329 cal domain size (Figure 1c, Figure 4a-d). This is consistent with the sensitivity of en-
330 trainment and detrainment to domain size (see Romps, 2014), both of which increase
331 as domains (and their updrafts) become smaller. Unlike detrainment and entrainment,
332 which display narrowing distributions across computational domain sizes as grid spac-
333 ing is increased, the distribution of relative humidity does not narrow—it only shifts to-
334 wards lower values. Jeevanjee and Zhou (2022) discuss the sensitivity of relative humid-
335 ity to horizontal resolution.

336 A higher relative humidity in small domains implies that convection is less efficient
337 at heating the atmosphere due to enhanced evaporation. This explains why the convective
338 mass flux is larger for small domains (Figure 1a, Figure 4e-h). High cloud fractions
339 are also larger in small domains (Figure 1b). This is likely contributed to by the larger

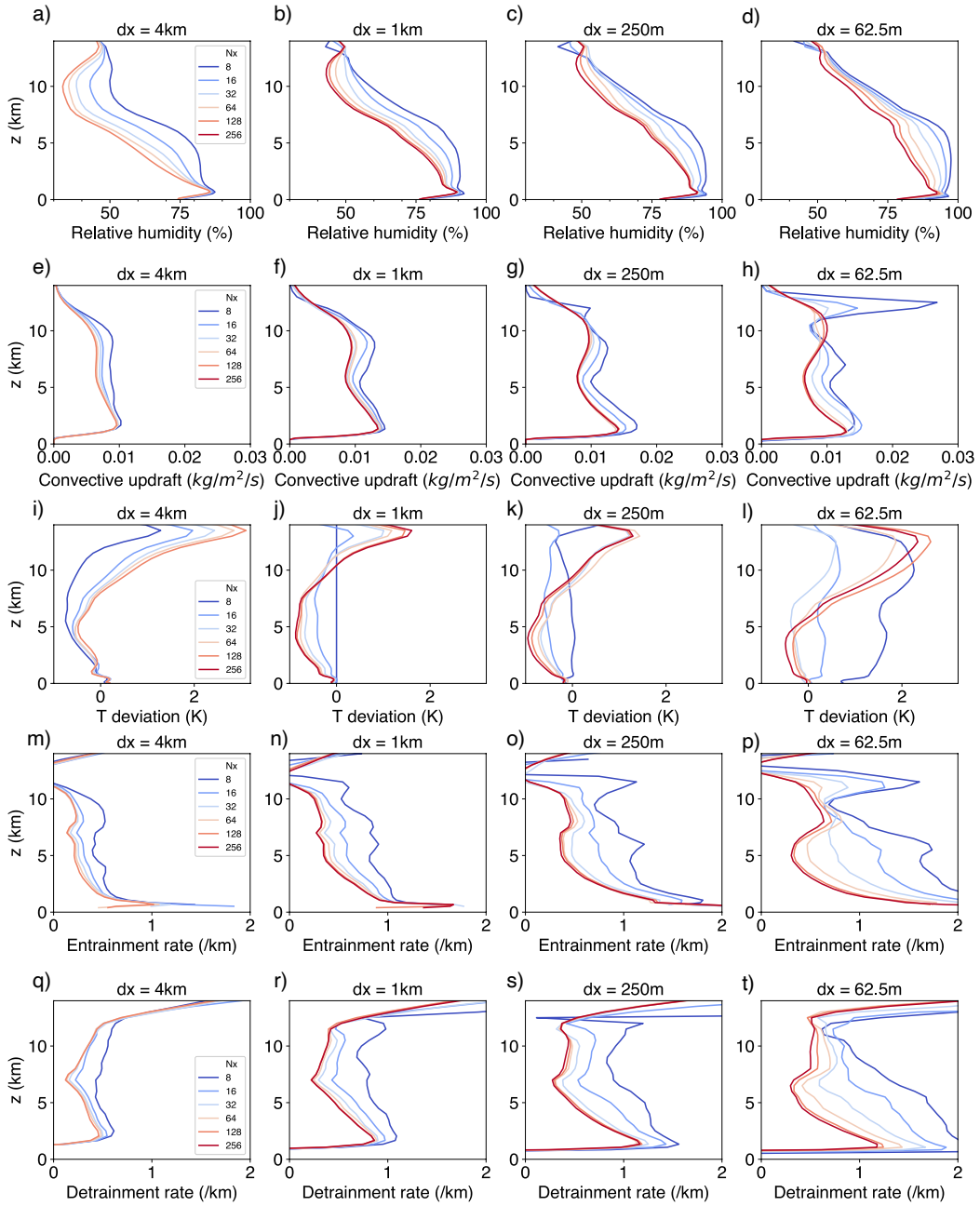


Figure 4. Sensitivity of domain mean profiles to computational domain size across horizontal resolutions of (left column), 1km (center left column), 250 m (center right column), and 62.5 m (right column). The rows from top-to-bottom are: (a-d) relative humidity, (e-h) updraft mass flux, (i-l) temperature deviation from $n_x=8$, (m-p) fractional entrainment rate, and (q-t) fractional detrainment rate. Entrainment and detrainment are diagnosed using the bulk plume model described in Section 2.2.

convective mass flux below the anvil level, which provides a larger anvil cloud source rate, as well as the higher relative humidity, which slows anvil cloud evaporation (Beydoun et al., 2021; Seeley et al., 2019). The change of temperature profiles may be viewed as mixture of two effects. On one hand, the stronger entrainment in the smaller domain tends to pull the temperature lapse rate away from moist pseudoadiabat lapse rate, making the temperature colder in smaller domain (Figure 4i). On the other, smaller domain also tends to have larger anvil cloud fraction and cloud radiative heating through the troposphere, which increases the temperature below anvil cloud in smaller domains (Figure 4j-l).

Figure 5 shows time series of precipitation, convective available potential energy (CAPE), and w_e . In addition to being higher, on average, the temporal variability of instability is also larger for small domains. The higher mean value of CAPE is a consequence of Equation (9): for small domains, the lapse rate needs to be larger (more unstable) to maintain a convective overturning circulation. In small domains, this manifests as periods of quiescence, when convection is suppressed, interspersed with periods of intense convection that occur when radiative cooling sufficiently steepens the lapse rate. In comparison, domain mean CAPE and precipitation are more consistent in time for large domains. This occurs, in part, because σ_c can be small in large domains, and consequently less instability is needed to maintain a convective circulation. The decreasing temporal variance with increasing computational domain size may also be contributed to by the increasing sample size.

4 Shallow convective cases

The heuristic argument of Section 3 hinges on the buoyancy condition that the rate of change of temperature in the convective region be larger than that of the subsiding non-convective region (Equation 6), and the implicit assumption that this condition must be satisfied in order for motion in the convective region to be ascending. While this is reasonable for deep convection, this may not capture the behavior of shallow convection as closely. For example, the boundary layer eddies that help maintain marine stratocumulus clouds are largely driven by strong radiative cooling at their tops (reviewed in Wood, 2012). Thus for completeness, we also tested the sensitivity of two shallow convective cases to computational domain size, described in Section 2.1. We used the BOMEX case to simulate trade cumulus, and we used the DYCOMS-RF01 case to simulate stratocumulus.

Figure 6 shows the 6-hour time series of cloud properties in the shallow convective simulations. Temporal variability for the small domains is much larger, likely due to the simulation only capturing the evolution of one or a small number of convective updrafts at a time. To enhance the signal-to-noise ratio of our results, we ran ensembles described in Section 2.1. The solid lines in Figure 6 represent the ensemble mean, while the shading represents the ensemble spread between the 25th to 75th quantiles. For both the BOMEX and DYCOMS-RF01 cases, the time evolution of cloud fraction and cloud water path converges for domains with at least 32×32 columns.

For the BOMEX case (Figure 6 left column), the smallest domain ($n_x=8$) shows significantly reduced cloud water path and slightly elevated cloud fraction compared to larger domains. These differences can also be viewed in the vertical profiles averaged over the last 2 hours (Figure 7). The updraft mass flux in $n_x=8$ has a very similar maximum value around 750 m but is shallower than the larger domains (Figure 7a). The faster decline of the updraft mass flux above the maximum indicates stronger detrainment (Figure 7d). This, taken together with the stronger diagnosed entrainment in $n_x=8$ (Figure 7c) is consistent with our result of stronger mixing for small domains from the deep convective simulations.

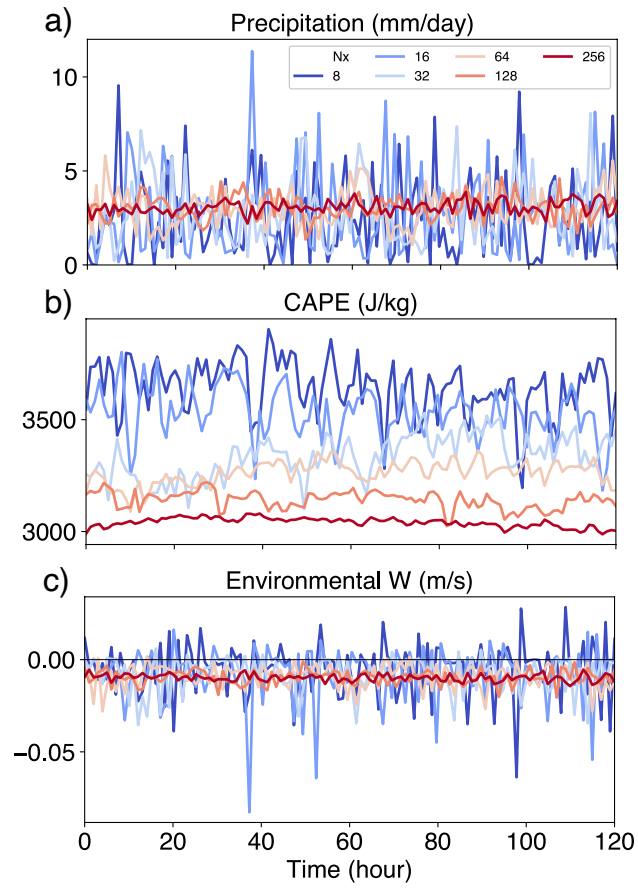


Figure 5. Time series of (a) surface precipitation, (b) convective available potential energy (CAPE), and (c) environmental vertical velocity across 5 days.

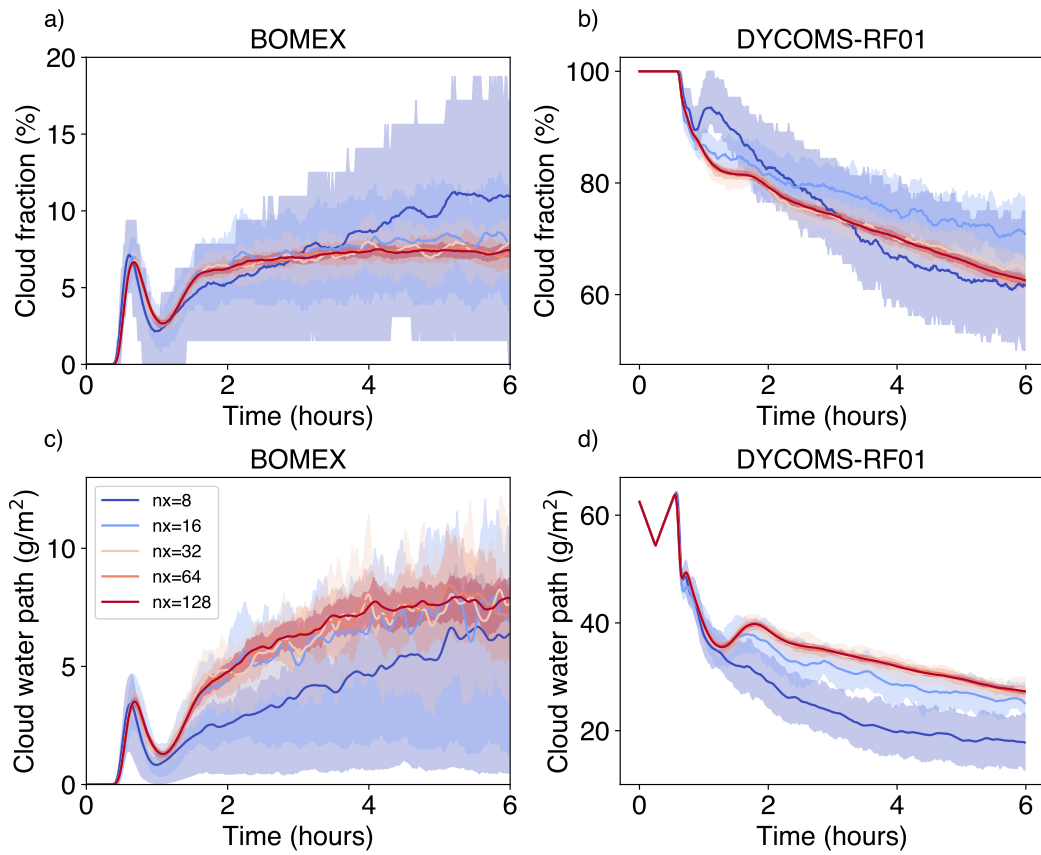


Figure 6. Time series of vertically integrated cloud fraction (top row) and cloud water path (bottom row) for the BOMEX case (left column) and the DYCOMS-RF01 case (right column). Solid lines are the ensemble mean, and the shading represents the 25th to 75th percentile of the ensemble spread. Cloud fraction here is defined as fraction of columns that have a cloud water path larger than 10 g m^{-2} .

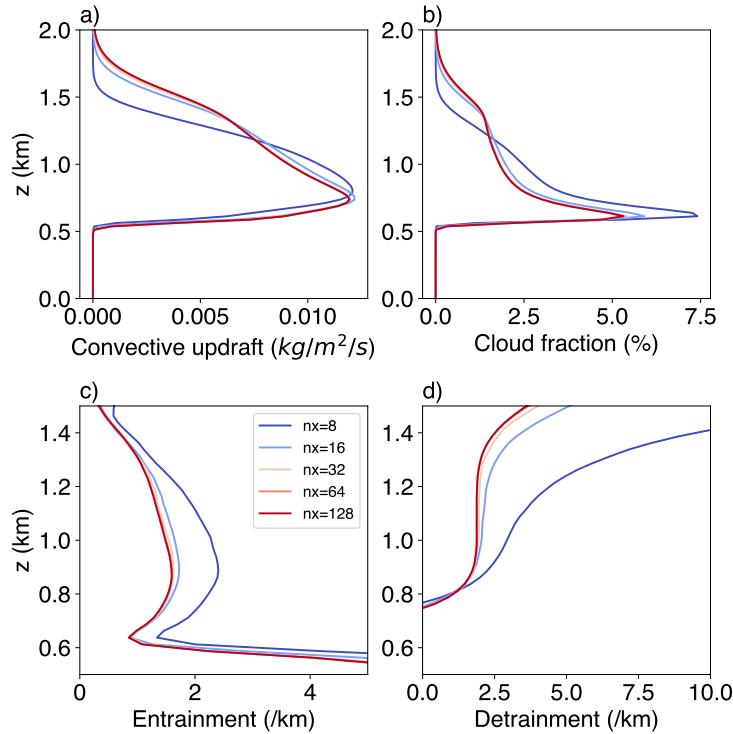


Figure 7. Mean atmosphere profiles over the last 2 hours in the BOMEX simulations: (a) updraft mass flux, (b) cloud fraction, (c) the fractional entrainment rate, and (d) the fractional detrainment rate. Entrainment and detrainment are diagnosed using the bulk plume model described in Section 2.2.

390 For the DYCOMS-RF01 stratocumulus case (Figure 6 right column), there is a sig-
 391 nificant reduction in the cloud water path for the two smaller domain sizes. For $nx=8$
 392 and $nx=16$, some ensemble members are able to sustain a larger cloud fraction than the
 393 larger domains. In $nx=8$, the stratocumulus cloud decks fully dissipate for some ensemble
 394 members (not shown). This may suggest that our smallest domain with 8×8 columns
 395 ($1\text{km} \times 1\text{km}$) is too small to sufficiently simulate stratocumulus and may trigger an in-
 396 stability that is sensitive to the initial noise perturbation. We encourage future studies
 397 to further explore this instability.

398 5 Summary

399 In simulations using convection resolving models (CRMs), small domains are used
 400 in both standalone simulations and within GCMs employing superparameterization or
 401 a multi-scale modeling framework. A CRM domain can be computationally small by hav-
 402 ing few grid columns, and it can also be physically small by representing a small phys-
 403 ical area.

404 Convective fractional area must be small in order to maintain positive buoyancy
 405 against a subsiding and warming environment. Small convective fractional area ensures
 406 that the downward mass flux is spread over a large area and hence, heats the environ-
 407 ment slowly. This is the same argument used to explain the observed smallness of the
 408 tropical convective ascent area (Bjerknes, 1938). In CRM domains, the smallest possi-
 409 ble convective fractional ascent area increases as the number of total grid columns de-
 410 creases. Consequently, convective fractional ascent area is forced to be large in CRM do-

411 mains with few grid columns and subsidence warming is strong, which suppresses con-
 412 vection. This argument is presented qualitatively in Pritchard et al. (2014).

413 Here, we present a heuristic argument to show why convection is “throttled”, or
 414 suppressed, in small domains. We show that

- 415 1. Small computational domains require more instability to sustain convection due
 416 to large convective fractional areas.
- 417 2. Physical updraft width is limited in both computationally and physically small
 418 domains, which increases updraft dilution by entrainment. This impact can be re-
 419 duced by increasing the grid spacing and by increasing the number of columns.
- 420 3. Detrainment occurs lower in the atmosphere for undilute convection in small do-
 421 mains. This is enhanced by the impact of domain size on updraft width and sub-
 422 sequent entrainment dilution.

423 As a result of “throttled” convection, the domain mean instability increases for small do-
 424 mains, and precipitation becomes more temporally variable, with periods of intense rain
 425 followed by relatively quiescent periods. Enhanced entrainment and detrainment in small
 426 domains increases the mean relative humidity, convective mass flux, and anvil cloud frac-
 427 tion. These conclusions are supported with CRM simulations of radiative convective equi-
 428 librium.

429 We also present results from shallow convective simulations across a range of do-
 430 main sizes for a shallow cumulus case and a marine stratocumulus case. In both cases,
 431 we see convergence of cloud properties when we increase the domain size. Similar to the
 432 deep convection simulations, the shallow cumulus simulations also show stronger en-
 433 trainment and detrainment rate in the small domains, leading to shallower updraft mass
 434 flux and cloud fraction. For the stratocumulus case, small domain seems to be more un-
 435 stable for cloud deck to maintain. This may suggest that it is insufficient to capture all
 436 the relevant processes for stratocumulus dynamics in a very small domain.

437 6 Discussion

438 An important new finding here is the suppression of convection that results from
 439 the limitation of updraft width by small domains, and subsequent strong entrainment
 440 dilution. This helps explain why simulated mean fields can still differ across larger do-
 441 mains, despite the expectation of convergent behavior beyond 32 columns for undiluted
 442 convection. We expect entrainment rates, and subsequent domain size sensitivity, to roughly
 443 converge at the domain size where the physical updraft width distribution is insensitive
 444 to domain size. In SAM, this occurs for domains with around 128×128 columns. Because
 445 this number is smaller for coarse grid spacing, we recommend using low horizontal res-
 446 olution for small computational domains simulating deep convection to avoid suppres-
 447 sion of deep convection. Additionally, the suggested domain sizes exhibiting convergence
 448 depend on entrainment and may be model dependent, as entrainment mixing relies, in
 449 part, on sub-grid schemes. Therefore, while all CRMs should show sensitivity to domain
 450 size, the precise size where convergence occurs could vary by model.

451 This study has direct implications for superparameterized modeling, which con-
 452 tinues to use computationally small domains because of the demanding computational
 453 cost. Pritchard et al. (2014) evaluate the climate of SP-GCM simulations with 8, 16, and
 454 32 columns in the embedded CRMs. A key result of their study was a stronger tropi-
 455 cal shortwave cloud forcing, which resulted from enhanced low-level liquid cloud and a
 456 drier and less cloudy upper troposphere. Also, the simulations with the smallest CRM
 457 domain produced more low intensity precipitation and less high intensity precipitation.
 458 These results differ from our results here. Our smallest domain simulations exhibit higher
 459 humidities throughout the troposphere, higher anvil cloud fractions, and a wider precip-

460 itation distribution. We hypothesize that these differences can be explained by circula-
 461 tions on the GCM grid that move energy between CRM domains in the SP setup. In an
 462 SP-GCM, convection can be continually suppressed in convectively stable regions because
 463 the CRM domain is not in energy balance. Conversely, in our simulations, the absence
 464 of a large-scale circulation means that convection has to happen somewhere in the do-
 465 main to balance radiative cooling.

466 The convective area fraction’s tight control by the domain lapse rate is in part a
 467 result of domain mass conservation ($\bar{w} = 0$). We can write the condition for convec-
 468 tion (6) because it is always true that environmental air is descending if there is convec-
 469 tion occurring. Consider however the case where $\bar{w} \neq 0$, for example in an SP-GCM where
 470 the CRM directly experiences the large-scale vertical motion of a host grid cell. Assum-
 471 ing condition (6) holds, (7) becomes

$$472 \quad \sigma_c < \frac{\Gamma_c - \Gamma_m - \frac{\bar{w}}{w_c}}{\Gamma_d - \Gamma_m + \Gamma_c - \Gamma_e}. \quad (12)$$

473 If $\bar{w} < 0$, condition (6) is still valid. However, convection may be less “throttled” be-
 474 cause the descending mean mass flux enables a larger maximum σ_c . That is, for a given
 475 computational domain size, convection may be triggered for less unstable profiles than
 476 is possible when \bar{w} *must* be zero. For large-scale ascent ($\bar{w} > 0$), environmental air is
 477 no longer guaranteed to be sinking and warming, and we can not claim (12) because of
 478 the potential for violation of condition (6). Currently, in both E3SM-MMF and SP-CESM,
 479 any large-scale vertical motion occurring on the GCM grid is communicated to the em-
 480 bedded CRM via a horizontally uniform forcing on the temperature (and moisture) ten-
 481 dencies (Grabowski, 2001), rather than on the velocity field. This does not impact the
 482 limitation of convective fractional ascent by the local lapse rate written in Equation (7).
 483 It remains to be seen if convective throttling is reduced in superparameterized simula-
 484 tions without strict enforcement of $\bar{w} = 0$.

485 Lastly, while quantitative, the argument we use to explain why a small CRM do-
 486 main “throttles” convection relies on a minimalist depiction of relations between vari-
 487 ables during convective motions. For example, radiation, which is not considered in our
 488 equations, may help reduce the critical lapse rate (Γ^*) needed to sustain an overturn-
 489 ing circulation for a given computational domain size because it heats the convective re-
 490 gion relative to the non-convective region and thus helps maintain condition (6). Sim-
 491 ilarly, we do not consider cooling in the environmental region due to evaporation of de-
 492 trained condensate, which may further help to reduce Γ^* . It is possible that these pro-
 493 cesses may have stronger effects than we anticipate. While entrainment is considered in
 494 a mostly qualitative sense in our discussion of the limitation of updraft width by domain
 495 size, we show in Figure 2 that it can have a large impact on Γ^* . Nonetheless, we believe
 496 that the model captures the primary relationships between variables that help explain
 497 convective throttling in small domains.

498 7 Data and Software Availability

499 Convection resolving model simulations were conducted with the System for At-
 500 mospheric Modeling (SAM) version 6.10.6 (M. Khairoutdinov, 2022).

501 Acknowledgments

502 This research has been supported by the National Oceanic and Atmospheric Adminis-
 503 tration Climate & Global Change Postdoctoral Fellowship Program through UCAR CPAESS
 504 Grant no. NA18NWS4620043B. This work used Bridges-2 at Pittsburgh Supercomput-
 505 ing Center through allocation EES230034 from the Advanced Cyberinfrastructure Co-
 506 ordination Ecosystem: Services & Support (ACCESS, Boerner et al., 2023) program, which
 507 is supported by National Science Foundation grants 2138259, 2138286, 2138307, 2137603,

508 and 2138296. We thank Zhiming Kuang, Kerry Emanuel, Xueying Yu, and Roger Samel-
509 son for helpful comments.

510 References

- 511 Beydoun, H., Caldwell, P. M., Hannah, W. M., & Donahue, A. S. (2021, August).
512 Dissecting anvil cloud response to sea surface warming. *Geophys. Res. Lett.*,
513 *48*(15).
- 514 Bjerknes, J. (1938). Saturated-adiabatic ascent of air through dry-adiabatically de-
515 scending environment. *Quart. J. Roy. Meteor. Soc.*, *64*, 325–330.
- 516 Boerner, T. J., Deems, S., Furlani, T. R., Knuth, S. L., & Towns, J. (2023, Septem-
517 ber). ACCESS: Advancing innovation: NSF’s advanced cyberinfrastructure
518 coordination ecosystem: Services & support. In *Practice and experience in
519 advanced research computing* (pp. 173–176). New York, NY, USA: Association
520 for Computing Machinery.
- 521 Grabowski, W. W. (2001, May). Coupling cloud processes with the Large-Scale dy-
522 namics using the Cloud-Resolving convection parameterization (CRCP). *J. At-
523 mos. Sci.*, *58*(9), 978–997.
- 524 Hannah, W. M., Jones, C. R., Hillman, B. R., Norman, M. R., Bader, D. C., Tay-
525 lor, M. A., . . . Lee, J. M. (2020, January). Initial results from the super-
526 parameterized E3SM. *J. Adv. Model. Earth Syst.*, *12*(1).
- 527 Hannah, W. M., Pressel, K., Ovchinnikov, M., & Elsaesser, G. (2022). Checker-
528 board patterns in E3SMv2 and E3SM-MMFv2. *Geoscientific Model Develop-
529 ment*, *15*(15), 6243–6257.
- 530 Holland, J. Z., & Rasmusson, E. M. (1973, January). Measurements of the atmo-
531 spheric mass, energy, and momentum budgets over a 500-kilometer square of
532 tropical ocean. *Mon. Weather Rev.*, *101*(1), 44–55.
- 533 Jeevanjee, N., & Zhou, L. (2022, March). On the resolution-dependence of anvil
534 cloud fraction and precipitation efficiency in radiative-convective equilibrium.
535 *J. Adv. Model. Earth Syst.*, *14*(3).
- 536 Khairoutdinov, M. (2022). *System for Atmospheric Modeling (version 6.10.6) [Soft-
537 ware]*. <http://rossby.msrc.sunysb.edu/~marat/SAM/>.
- 538 Khairoutdinov, M. F., & Randall, D. A. (2001, September). A cloud resolving model
539 as a cloud parameterization in the NCAR community climate system model:
540 Preliminary results. *Geophys. Res. Lett.*, *28*(18), 3617–3620.
- 541 Khairoutdinov, M. F., & Randall, D. A. (2003, February). Cloud resolving modeling
542 of the ARM summer 1997 IOP: Model formulation, results, uncertainties, and
543 sensitivities. *J. Atmos. Sci.*, *60*(4), 607–625.
- 544 Kuang, Z., & Bretherton, C. S. (2006). A mass-flux scheme view of a high-resolution
545 simulation of a transition from shallow to deep cumulus convection. *Journal of
546 the Atmospheric Sciences*, *63*(7), 1895–1909.
- 547 Lin, G., Jones, C. R., Leung, L. R., Feng, Z., & Ovchinnikov, M. (2022, January).
548 Mesoscale convective systems in a superparameterized E3SM simulation at
549 high resolution. *J. Adv. Model. Earth Syst.*, *14*(1).
- 550 Liu, N., Pritchard, M. S., Jenney, A. M., & Hannah, W. M. (2023, April). Un-
551 derstanding precipitation bias sensitivities in E3SM-multi-scale modeling
552 framework from a dilution framework. *J. Adv. Model. Earth Syst.*, *15*(4).
- 553 Morrison, H. (2017, March). An analytic description of the structure and evolution
554 of growing deep cumulus updrafts. *J. Atmos. Sci.*, *74*(3), 809–834.
- 555 Morrison, H., Peters, J. M., Varble, A. C., Hannah, W. M., & Giangrande, S. E.
556 (2020, October). Thermal chains and entrainment in cumulus updrafts. part i:
557 Theoretical description. *J. Atmos. Sci.*, *77*(11), 3637–3660.
- 558 Muller, C. J., & Held, I. M. (2012, August). Detailed investigation of the Self-
559 Aggregation of convection in Cloud-Resolving simulations. *J. Atmos. Sci.*,
560 *69*(8), 2551–2565.

- 561 Patrizio, C. R., & Randall, D. A. (2019, July). Sensitivity of convective self-
 562 aggregation to domain size. *J. Adv. Model. Earth Syst.*, *11*(7), 1995–2019.
- 563 Peng, L., Pritchard, M., Blossey, P. N., Hannah, W. M., Bretherton, C. S., Terai,
 564 C. R., & Jenney, A. M. (2023). Improving stratocumulus cloud amounts in a
 565 200-m resolution multi-scale modeling framework through tuning of its interior
 566 physics. *ESS Open Archive*.
- 567 Peng, L., Pritchard, M., Hannah, W. M., Blossey, P. N., Worley, P. H., & Brether-
 568 ton, C. S. (2022, May). Load-balancing intense physics calculations to embed
 569 regionalized high-resolution cloud resolving models in the E3SM and CESM
 570 climate models. *J. Adv. Model. Earth Syst.*, *14*(5).
- 571 Pritchard, M. S., Bretherton, C. S., & DeMott, C. A. (2014, September). Restricting
 572 32-128 km horizontal scales hardly affects the MJO in the superparameterized
 573 community atmosphere model v.3.0 but the number of cloud-resolving grid
 574 columns constrains vertical mixing. *J. Adv. Model. Earth Syst.*, *6*(3), 723–739.
- 575 Romps, D. M. (2014, October). An analytical model for tropical relative humidity.
 576 *J. Clim.*, *27*(19), 7432–7449.
- 577 Seeley, J. T., Jeevanjee, N., Langhans, W., & Romps, D. M. (2019, January). For-
 578 mation of tropical anvil clouds by slow evaporation. *Geophys. Res. Lett.*,
 579 *46*(1), 492–501.
- 580 Siebesma, A. P., Bretherton, C. S., Brown, A., Chlond, A., Cuxart, J., Duynkerke,
 581 P. G., ... Others (2003). A large eddy simulation intercomparison study of
 582 shallow cumulus convection. *J. Atmos. Sci.*, *60*(10), 1201–1219.
- 583 Stevens, B., Moeng, C.-H., Ackerman, A. S., Bretherton, C. S., Chlond, A., de
 584 Roode, S., ... others (2005). Evaluation of large-eddy simulations via obser-
 585 vations of nocturnal marine stratocumulus. *Monthly weather review*, *133*(6),
 586 1443–1462.
- 587 Wing, A. A., Reed, K. A., Satoh, M., Stevens, B., Bony, S., & Ohno, T. (2018,
 588 March). Radiative–convective equilibrium model intercomparison project.
 589 *Geoscientific Model Development*, *11*(2), 793–813.
- 590 Wing, A. A., Stauffer, C. L., Becker, T., Reed, K. A., Ahn, M., Arnold, N. P., ...
 591 Zhao, M. (2020, July). Clouds and convective Self-Aggregation in a Multi-
 592 Model ensemble of Radiative-Convective equilibrium simulations. *J. Adv.*
 593 *Model. Earth Syst.*
- 594 Wood, R. (2012, August). Stratocumulus clouds. *Mon. Weather Rev.*, *140*(8), 2373–
 595 2423.
- 596 Yanase, T., Nishizawa, S., Miura, H., Takemi, T., & Tomita, H. (2020, August).
 597 New critical length for the onset of self-aggregation of moist convection. *Geo-*
 598 *phys. Res. Lett.*, *47*(16).

On the dependence of simulated convection on domain size

A. M. Jenney¹, Z. Hu²

¹College of Earth, Ocean, and Atmospheric Sciences, Oregon State University

²Department of Earth and Planetary Sciences, Harvard University

Key Points:

- Deep convection is suppressed in domains with few grid columns due to strong subsidence warming and entrainment into small updrafts
- This effect can be reduced by increasing grid spacing
- Small domains are more humid than large domains regardless of grid spacing because of enhanced convective mixing

Corresponding author: Zeyuan Hu, zeyuan.hu@fas.harvard.edu

Corresponding author: Andrea Jenney, andrea.jenney@oregonstate.edu

12 Abstract

13 We present a heuristic model to quantitatively explain the suppression of deep con-
 14 vection in convection-resolving models (CRMs) with small domains. We distinguish be-
 15 tween “computational” smallness (few grid columns) and “physical” smallness (repre-
 16 senting a small geographic area). Domains that are computationally small require greater
 17 instability to sustain convection because they force a large convective fraction, driving
 18 strong compensating subsidence warming. Consequently, detrainment occurs lower for
 19 undiluted convection. Both computationally and physically small domains limit the phys-
 20 ical updraft width, increasing entrainment dilution. This enhancement of entrainment
 21 strengthens the sensitivity to domain size beyond that for undiluted deep convection.
 22 Coarsening grid spacing to expand the physical domain and physical updraft width can
 23 reduce domain size sensitivity. Simulations using the System for Atmospheric Model-
 24 ing (SAM) confirm the heuristic model results. We also present simulation results for
 25 two shallow convection cases, which are less sensitive to domain size, but also exhibit sen-
 26 sitivities.

27 Plain Language Summary

28 We present a simple mathematical model that helps explain why cloudy upward
 29 air movement (convection) is suppressed in “small” computer simulations used for study-
 30 ing weather. We look at two types of “smallness”: one is about the computer’s limita-
 31 tions (fewer grid columns), and the other is about how big the area that is being rep-
 32 resented would be on a map (physical size). When the computer model has fewer columns,
 33 more energy is needed for upward air movement because the compressive warming of sink-
 34 ing air around clouds is stronger. This affects where air stops moving upward (detrain-
 35 ment).

36 Both types of smallness make the upward air column narrower in a physical sense,
 37 causing more outside air to mix in (entrainment). Because cloudy air is typically warmer
 38 and more humid than the air around it, this mixing reduces the temperature of the cloudy
 39 air and weakens the upward air movement. We found that increasing the number of columns
 40 or making the columns wider can help reduce these effects. We tested this in simulations
 41 and our results support our simple mathematical model.

42 1 Introduction

43 Convection-resolving models (CRMs) are popular tools used to simulate large-scale
 44 turbulent motions associated with clouds and convection. In stand-alone simulations, CRMs
 45 are oftentimes run with domains as small as 100 km to inhibit the spontaneous cluster-
 46 ing of the convective region in a phenomenon known as convective self aggregation (e.g.,
 47 Wing et al., 2018, 2020), which occurs preferentially in larger domains (Muller & Held,
 48 2012; Yanase et al., 2020). In addition, small CRM domains are often used in general
 49 circulation models (GCMs) employing superparameterization (SP), also known as multi-
 50 scale modeling framework (MMF), in which the convective parameterization is replaced
 51 with many embedded CRMs. Recent SP/MMF simulations use CRMs with as few as
 52 64 columns to reduce computational cost (e.g., Hannah et al., 2020, 2022; Lin et al., 2022).

53 Many studies exploring the sensitivity of standalone CRM simulations to domain
 54 size focus on convective self aggregation (Muller & Held, 2012; Patrizio & Randall, 2019;
 55 Yanase et al., 2020). These studies have shown that convective self-aggregation tends
 56 to occur at domain sizes larger than 200 km. In CRM simulations forced with observa-
 57 tions M. F. Khairoutdinov and Randall (2001) find that the precipitable water increased
 58 and rainfall fraction decreased with increasing domain size. However, these simulations

59 varied in dimensionality, horizontal resolution, and vertical resolution, so inferring the
60 isolated impacts of varying domain size is not possible.

61 Sensitivity to CRM domain size has also been studied in modern SP setups. Liu
62 et al. (2023) compare 2-D simulations of the Energy Exascale Earth System Model-MMF
63 (E3SM-MMF) with 32 total columns to 3-D simulations with 32 grid columns in each
64 horizontal dimension (1024 total columns) and find large differences in mean precipita-
65 tion and its statistics over some tropical regions. Whether the differences were driven
66 entirely by differences in domain size in the CRMs or by their dimensionality is unclear.
67 Peng et al. (2022) find differences in cloud fractions up to 0.4 and absorbed shortwave
68 radiation up to 60 W m^{-2} in some regions when comparing E3SM-MMF simulations with
69 32 vs. 64 CRM columns. E3SM-MMF with 2D CRMs with high horizontal resolution
70 (200 m) but small domains (12.8 km) appeared to under-resolve larger eddies important
71 for marine boundary layer clouds (Peng et al., 2023). As in other studies, the different
72 horizontal resolutions associated with different CRM domain sizes of Peng et al. (2022)
73 and Peng et al. (2023) makes disentangling the effects of domain size from horizontal res-
74 olution a challenge.

75 Few studies have explicitly studied the isolated impact of CRM domain size inde-
76 pendent of horizontal resolution on convective behavior and the mean atmospheric state
77 for the small domain sizes used in SP models. Pritchard et al. (2014) found that decreas-
78 ing the CRM domain size from 32 to 8 columns (while keeping horizontal resolution con-
79 stant) led to an increase in the climate sensitivity of an SP GCM, primarily due to changes
80 in low-level cloudiness. They propose a convective “throttling” hypothesis grounded in
81 buoyancy, in which small CRM domains limit the frequency that deep convection can
82 occur because of strong warming by compensating subsidence occurring over a fraction-
83 ally smaller area than is possible in a large CRM domain. This occurs because the min-
84 imum updraft size is limited by the fraction of the domain occupied by a single grid col-
85 umn, which increases as the number of grid columns decreases. As a result of convec-
86 tive throttling, the lower troposphere remains less ventilated in small CRM domains, re-
87 sulting in increased lower tropospheric humidity, denser liquid clouds, and a cooler up-
88 per troposphere. Despite these differences, the mean tropical radiative cooling rate is in-
89 sensitive to domain size, which implies a broader distribution of simulated deep convec-
90 tion at the smallest CRM scales due to infrequent yet intense deep convection needed
91 to balance the radiative cooling. These ideas can be traced back to Bjerknes (1938), who
92 provided a similar argument to explain the observed smallness of the tropical updraft
93 fraction.

94 Despite these advances, a *quantitative* understanding of the mechanisms of the rela-
95 tionship between domain size and mean atmospheric properties remains limited. For
96 example, the domain size at which convergence occurs and how domain size sensitivi-
97 ties interact with horizontal resolution sensitivities (e.g., Jeevanjee & Zhou, 2022) both
98 remain unclear. Motivated by the fact that small domain CRM simulations continue to
99 be run both as standalone simulations and in SP GCMs, this study aims to quantita-
100 tively explore the mechanisms proposed in Pritchard et al. (2014) using CRM experi-
101 ments (i.e., without the host GCM) with relatively “small” domain sizes (i.e., domain
102 sizes smaller than required for convective self-aggregation).

103 2 Methods

104 2.1 Experimental Setup

105 We use the System for Atmosphere Modeling (SAM; Khairoutdinov and Randall
106 2003), version 6.10.6, configured as a cloud-resolving model. A simple Smagorinsky-type
107 scheme (M. F. Khairoutdinov & Randall, 2003) computes sub-grid scale momentum and
108 scalar tendencies. We run both deep and shallow convective cases.

109 All deep convective simulations use 60 vertical levels with a model top located near
 110 26km and a rigid-lid top boundary condition. The vertical grid spacing linearly increases
 111 from 75m near the surface up to 2.5km, above which it is held constant at 500m. A sponge
 112 layer is located above 18km. The radiation scheme is the Rapid and Accurate Radia-
 113 tive Transfer Model for General Circulation Models (RRTMG) (Iacono et al. 2008). We
 114 use a constant solar insolation (no diurnal cycle) with fixed solar constant of 683.5 W
 115 m⁻² and zenith angle of 50.5°. Domain-averaged horizontal wind is nudged to zero at each
 116 vertical level with a nudging time scale of 1 hr. Sea surface temperature is fixed uniformly
 117 at 303K. Deep convective simulations are initialized from predefined initial temperature
 118 and moisture profiles and spun up for 100 days. White noise temperature perturbations
 119 on the order of 0.01K are applied to the lowest 5 model layers to initialize convection.
 120 Unless otherwise noted, a 20-day period after spin-up is used to compute equilibrium statis-
 121 tics. Domain-mean statistics are sampled every 2 min and then averaged to estimate hourly
 122 domain-mean statistics. Instantaneous 3-D fields are saved every 30 minutes.

123 We present results from 3-D deep convective simulations with 1 km horizontal resolu-
 124 tion and 8, 16, 32, 64, 128, 256 grid cells in each horizontal direction (“nx”). To ex-
 125 plore interactions between domain size and horizontal resolution sensitivity, we further
 126 ran 3 additional sets of simulations with 4km, 250m, and 62.5m resolution. For complete-
 127 ness, we also ran two-dimensional simulations with 16 and 128 columns, which we omit
 128 results from because of their close similarity to the 3-D runs.

129 For shallow convective simulations, We used large scale forcings, boundary condi-
 130 tions, and initial profiles from two field studies: the Barbados Oceanographic and Me-
 131 teorological EXperiment (BOMEX) (Holland & Rasmusson, 1973) as in Siebesma et al.
 132 (2003) to simulate shallow cumulus (“trade” cumulus) and the first research flight of the
 133 second Dynamics and Chemistry of Marine Stratocumulus (DYCOMS-RF01) (Stevens
 134 et al., 2005) to simulate marine stratocumulus. For these shallow convection simulations,
 135 we used a fixed horizontal resolution of 125 m and a fixed vertical resolution of 25 m with
 136 128 vertical levels. The DYCOMS-RF01 simulations are initialized with the same white
 137 noise temperature perturbation method as the deep convective simulations. The BOMEX
 138 simulations were initialized with white noise temperature perturbations on the order of
 139 0.1 K and water vapor perturbations on the order of 0.025 g kg⁻¹ applied to the low-
 140 est 1.6 km. Shallow convection simulations were run for 6 hours with a time step of 2
 141 seconds. Unlike the deep convective simulations, here we turned off precipitation. We
 142 do not include radiation in the BOMEX simulation, and use a simple interactive long-
 143 wave radiation calculation as in Stevens et al. (2005) for DYCOMS-RF01. We present
 144 results with 8, 16, 32, 64, 128 grid cells in each horizontal direction. Domain-mean statis-
 145 tics are sampled every 20 seconds and then averaged to estimate minute-mean domain-
 146 mean statistics.

147 We ran ensembles of the shallow convective cases to enhance the signal to noise ra-
 148 tio. These ensembles were initialized using different random numbers for the initial white
 149 noise perturbation. Most simulations have 64 ensemble members. However, for specific
 150 cases, we adjusted the number of members: we present 1024 members for the nx=8 BOMEX
 151 case, and 256 members for the nx=16 BOMEX and the nx=16 DYCOMS-RF01 cases.

152 **2.2 Methods for diagnosing entrainment and detrainment rate**

153 In later sections, we will present some results relating to diagnosed fractional en-
 154 trianment and detrainment rate. Here we document how they are calculated. We first
 155 estimate the entrainment and detrainment rate through a simple entraining-detraining
 156 bulk-plume model:

$$157 \frac{\partial \phi_u}{\partial z} = -\epsilon(\phi_u - \phi_n) + S_u \quad (1)$$

$$158 \frac{1}{M} \frac{\partial M}{\partial z} = \epsilon - \delta \quad (2)$$

159

160 where ϕ is a relatively conserved variable, subscripts “u” and “n” denote averages across
 161 convective updraft grid cells and non-updraft grid cells, S_u is the net source of ϕ within
 162 updraft, ϵ and δ represent the fractional entrainment rate and detrainment rates, and
 163 M represents the convective updraft mass flux. Here, we define ϕ_u as the water vapor
 164 plus cloud water mixing ratio. S_u is evaporation of precipitation minus cloud-to-precipitation
 165 conversion averaged across updraft grid cells, and is zero for our shallow convection sim-
 166 ulations where we turned off precipitation. Convective updraft grid cells are those with
 167 cloud mixing ratios greater than 10^{-5} kg kg $^{-1}$ and upward vertical velocities greater than
 168 1 m s $^{-1}$. Non-updraft grid cells are defined as those with cloud water mixing ratios smaller
 169 than 10^{-5} kg kg $^{-1}$. Horizontally averaged ϕ_u , ϕ_n , S_u , and M were saved as part of our
 170 domain-mean statistics outputs.

171 In addition to the above single plume model, we also used a spectrum plume method
 172 to diagnose entrainment rate distribution (Kuang & Bretherton, 2006). Unlike the sin-
 173 gular plume model which assumes all the updrafts have the same entrainment rate profile,
 174 the spectrum plume model allows updrafts to have a spectrum of entrainment rates. Here
 175 we briefly describe the procedure of calculating entrainment rate distribution used in (Kuang
 176 & Bretherton, 2006). First we need to calculate the convective updraft mass flux dis-
 177 tribution in the space of frozen moist static energy (FMSE) and height. FMSE is defined
 178 as $c_p T + gz + L_v q - L_f q_i$. Then we can specify a set of fractional entrainment rate val-
 179 ues, and calculating the FMSE profile of an entraining plume using the mean FMSE in
 180 the updraft at the cloud base for each fractional entrainment rate. Then, at each level,
 181 we can count how many mass flux falls into each entrainment rate interval according to
 182 their FMSE. Essentially we get mass flux distribution in the space of entrainment rate
 183 and height.

184 3 Domain “smallness” and its impacts

185 Domain size has a clear impact on mean state quantities of limited-domain CRM
 186 simulations. For deep convective simulations, Figure 1a-c shows mean profiles of con-
 187 vective mass flux, cloud fraction, and relative humidity, each of which decrease through-
 188 out the troposphere with increasing domain size. Larger domains are also colder below
 189 10 km, and warmer above (Figure 1d).

190 A CRM domain may be small in two ways: it may be computationally small by
 191 having few grid columns, and it also may be physically small by covering a small phys-
 192 ical area. Increasing the horizontal grid spacing increases the physical domain size of a
 193 computationally fixed domain size (i.e., fixed number of grid columns). In the discus-
 194 sion that follows, we will present a heuristic argument to explain how computational small-
 195 ness leads to convective throttling and how this may be partially compensated by increas-
 196 ing the physical domain size.

197 The net circulation over a limited domain is the sum of the convective and envi-
 198 ronmental mass fluxes,

$$199 \quad \bar{w} = w_c \sigma_c + w_e \sigma_e, \quad (3)$$

200 where w is vertical velocity, σ is the fractional area of convection (subscript c) and en-
 201 vironment (subscript e), and the over bar indicates a domain mean quantity. In writ-
 202 ing (3), we have ignored any horizontal variation in density. In both SP-CESM and E3SM-
 203 MMF, $\bar{w} = 0$ throughout the CRM domain. We thus omit \bar{w} from subsequent equa-
 204 tions.

205 If environmental air is sinking ($w_e < 0$), it warms due to adiabatic compression
 206 at the rate given by $w_e(\Gamma_e - \Gamma_d)$, where $\Gamma = -\partial T/\partial z$ is the lapse rate and Γ_d is the
 207 dry adiabatic lapse rate. Using Equation (3) and the fact that the fractional areas of con-

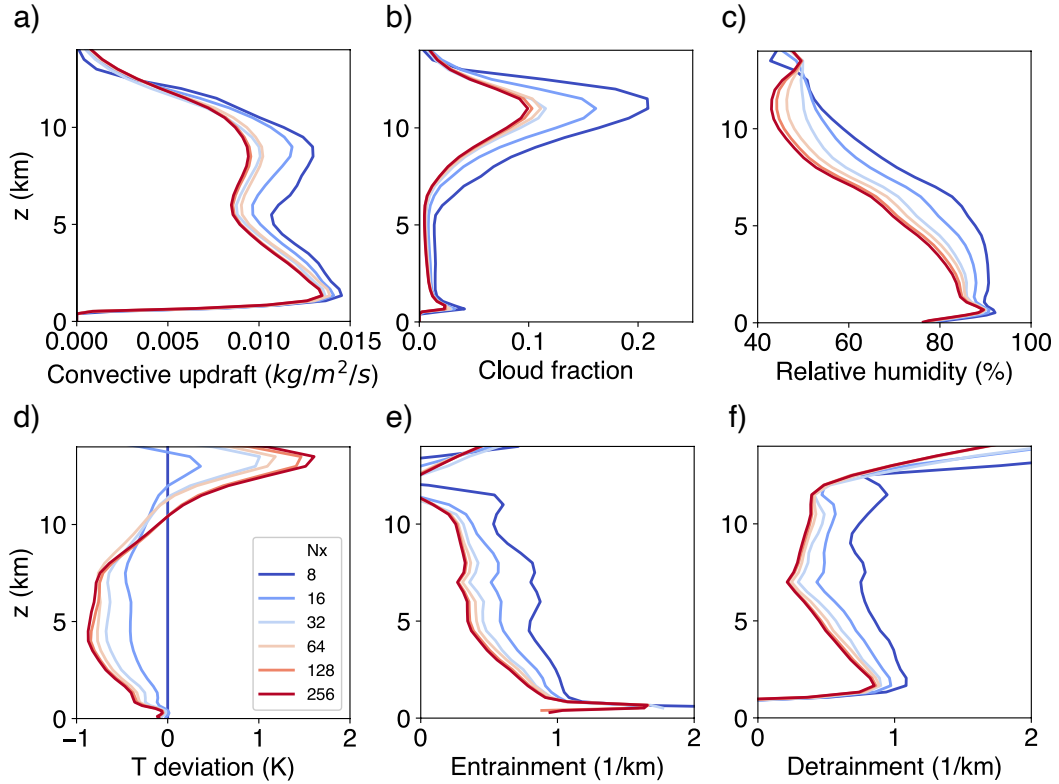


Figure 1. Dependence of atmospheric profiles on domain size for deep convective simulations: (a) updraft mass flux, (b) cloud fraction, (c) relative humidity, (d) temperature deviation from $n_x=8$, (e) fractional entrainment rate and (f) fractional detrainment rate. Entrainment and detrainment are diagnosed using the bulk plume model described in Section 2.2.

vection and of the environment must sum to one, we can write subsidence warming in the descent region as

$$\frac{dT_e}{dt} = -\frac{w_c \sigma_c}{1 - \sigma_c} (\Gamma_e - \Gamma_d). \quad (4)$$

The rate that temperature changes in the ascent region during undilute moist convection is

$$\frac{dT_c}{dt} = w_c (\Gamma_c - \Gamma_m), \quad (5)$$

where Γ_m is the saturated adiabatic lapse rate. To sustain a buoyancy-driven convective overturning circulation, positive buoyancy of the convective region is required. This means that the convective region must maintain a positive virtual temperature difference from the surrounding, descending environment. We can approximate this condition as

$$\frac{dT_c}{dt} > \frac{dT_e}{dt}, \quad (6)$$

which we can re-write in terms of the ascent area using Eqs. (4) and (5) as,

$$\sigma_c < \frac{\Gamma_c - \Gamma_m}{\Gamma_d - \Gamma_m + \Gamma_c - \Gamma_e}. \quad (7)$$

Equation (7) describes a limit on the maximum possible fractional convective area in a limited-domain CRM with no mean circulation by the lapse rates of the convective and non-convective region. The largest σ_c that can exist during ongoing convection increases with the instability of the convective region (Γ_c). Conversely, convective area is limited when instability is small. This is a consequence of condition (6). Because subsidence warming is stronger for faster sinking motion, small ascent areas ensure that subsidence warming is weak by being spread over a large area (Bjerknes, 1938). Second, in addition to the instability of the convective region, Equation (7) also shows that horizontal temperature gradients exert a limit on σ_c . When $\Gamma_c - \Gamma_e$ is large, environmental air is more likely to be warmer than convective region air. Thus, convective area must be small for large $\Gamma_c - \Gamma_e$ to keep w_e small and maintain positive convective region buoyancy. In CRM domains using superparameterized models, this effect may be second-order due to the relative smallness of CRM domains and the resulting closeness of Γ_c and Γ_e . For $\Gamma_c \approx \Gamma_e = \bar{\Gamma}$, Equation (7) simplifies to

$$\sigma_c < \frac{\bar{\Gamma} - \Gamma_m}{\Gamma_d - \Gamma_m}. \quad (8)$$

3.1 Small computational domains require more instability to sustain convection

We thus arrive at the first way that small computational CRM domains “throttle” convection. Computational domain size limits the minimum value that σ_c can assume: The smallest possible value of σ_c in a CRM domain is $1/N$ where N is the number of grid columns. This number decreases as the computational domain size and the number of grid columns increases.

For $\Gamma_c \approx \Gamma_e$ (a close approximation in a small domain), the threshold instability (Γ^*) at which a sustained convectively-driven overturning circulation is supported given a minimum possible σ_c (σ_c^*) can be inferred from Equation (8) as:

$$\Gamma^* > \sigma_c^* (\Gamma_d - \Gamma_m) + \Gamma_m \quad (9)$$

Equation (9) shows that as the computational domain size increases and σ_c^* decreases, Γ^* also decreases. As σ_c^* approaches zero, Γ^* approaches Γ_m . Figure 2 shows Γ^* computed from Equation (9) for domains with computational sizes ranging from 2 columns to 512 columns. For undilute convection (solid lines), this critical instability converges for domains larger than about 32 columns (a common number for SP simulations).

Buoyant convection doesn't occur without entrainment. Equation (5) can be modified for entraining convection as

$$\frac{dT_c}{dt} = w_c(\Gamma_c - \Gamma_m - \epsilon\beta) \quad (10)$$

where ϵ is the fractional entrainment rate and β is a dilution factor that depends on the difference in temperature and humidity between the updraft air and the entrained air, which we will crudely approximate as

$$\beta = T_c - T_e + \frac{L_v}{c_p}(q_s - q_e). \quad (11)$$

In Equation (11), L_v is the latent heat of vaporization, c_p is the specific heat capacity of dry air, and q is the water vapor mixing ratio. In writing (11), we have assumed that the entrained air has the temperature and humidity of the environment and that the convective region is saturated (q_s). We have also neglected differences in latent heating due to ice processes.

When the effects of entrainment are considered in the dependence of Γ^* on domain size, convergence at large domain sizes diminishes. We illustrate this with an example in Figure 2, which shows Γ^* profiles computed using a modification of Equation (9) that includes entrainment with (10) and (11). We neglect temperature differences between the convective and non-convective region ($T_c - T_e = 0$). We apply a 1% decrease in the relative humidity for successive domain sizes (as in Figure 1c), and entrainment rates which decrease by 5% as the number of columns is doubled (as in Figure 1e; see Section 3.2). Figure 2 shows that incorporating the impact of entrainment on Γ^* reduces large domain size convergence. This is a consequence of the sensitivity of the entrainment rate to domain size (which we discuss in the next section), despite a contribution in the opposite direction by the spread in relative humidity with domain size.

In summary, one way small computational domains “throttle” convection is by requiring more instability to sustain convection due to large σ_c . As we will show in the next section, entrainment rates also decrease as domain size decreases. As a result, while there is convergent behavior in Γ^* for domains larger than 32 columns for undilute convection, differences in entrainment reduce this convergence, and differences in Γ^* with domain size exist even for computationally large domains.

3.2 Small domains limit updraft width and enhance convective mixing

The critical instability in Equation (9) is the threshold lapse rate for *one grid column* to buoyantly convect without violating condition (6). For a given value of $\Gamma > \Gamma^*$, the number of grid columns available for convection increases with the computational domain size. This implies, for a fixed grid size, that increasing the total number of columns also allows updrafts to be *physically* wider. Convective entrainment rates are larger for physically small updrafts (Morrison, 2017; Morrison et al., 2020). Thus, the second way that CRM domain size “throttles” convection is by limiting updraft width and reducing updraft buoyancy by enhancing dilution by entrainment.

Our simulations are consistent with this behavior. Figure 1e shows that the mean fractional entrainment rate decreases with increasing computational domain size (for a fixed grid spacing). This occurs because updrafts are forced to be physically small in small domains. Figure 3 shows distributions of entrainment rate and updraft width at 8 km

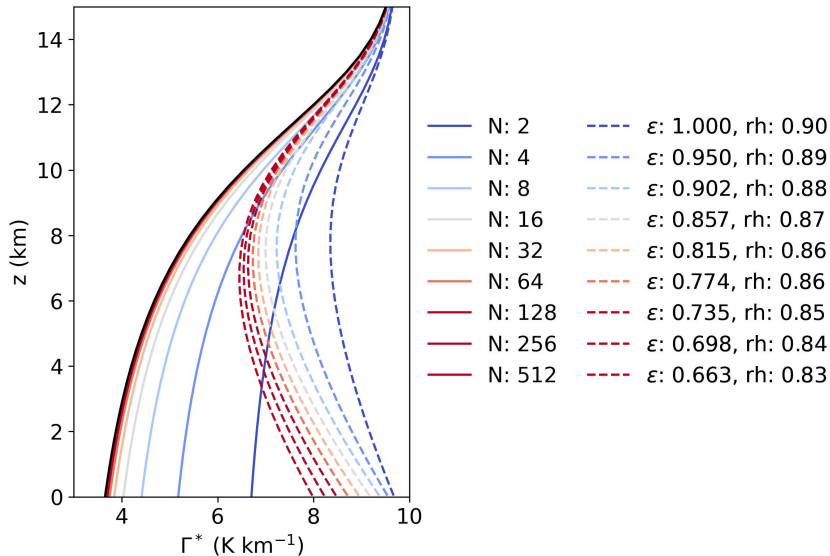


Figure 2. The critical lapse rate, Γ^* , needed to sustain a convective overturning circulation from Equation (9) for domains of different computational sizes. Here, “N” refers to the total number of grid columns. Solid lines show Γ^* for undilute convection. Dashed lines show Γ^* when idealized entrainment dilution is considered. Entrainment rates and relative humidities, which vary with the number of columns, (km^{-1}) are shown in the legend. Black line is the moist adiabatic lapse rate for a surface temperature of 300 K.

295 for square domains with 16, 64, and 256 columns in each horizontal dimension. As
 296 expected, updrafts are narrower in the small domain and entrainment rates are larger.
 297 The other two domain sizes are more similar, yet exhibit differences in line with our ex-
 298 pectations: the largest domain has slightly larger updrafts and slightly weaker entrain-
 299 ment rates.

300 For a small domain (such that $\sigma_c \approx \sigma_c^*$) at a computationally fixed size, increas-
 301 ing the grid spacing will make updrafts physically wider. Thus, we expect that they should
 302 also entrain less (Morrison, 2017; Morrison et al., 2020). Additional simulations with vary-
 303 ing horizontal resolution corroborate this expectation. Figure 4m-p shows entrainment
 304 rates for simulations with a range of computational domain sizes as grid spacing is de-
 305 creased from 4 km (left) to 62.5 m (right). As the grid spacing decreases and updrafts
 306 become smaller, the distribution of entrainment rates shifts towards larger values. Dif-
 307 ferences in the entrainment rate between resolutions are largest for the smallest domain.

308 In summary, computationally small domains increase convective entrainment rates
 309 because they limit updraft width. This impact can be reduced either by increasing the
 310 physical or computation domain size.

311 3.3 Convection in small domains detrains lower

312 Computationally small domains limit the minimum possible value that σ_c can as-
 313 sume. As a result of σ_c that is forced to be large, updrafts are inhibited by too-strong
 314 compensating subsidence (Section 3.1). In Section 3.2, we discussed how domain size lim-
 315 its updraft width, and enhances entrainment. It can be intuited that detrainment should
 316 also occur lower in small domains as a result of these combined effects. This is confirmed
 317 in our simulations. Figures 1f and 4q-t show that detrainment in simulated convection

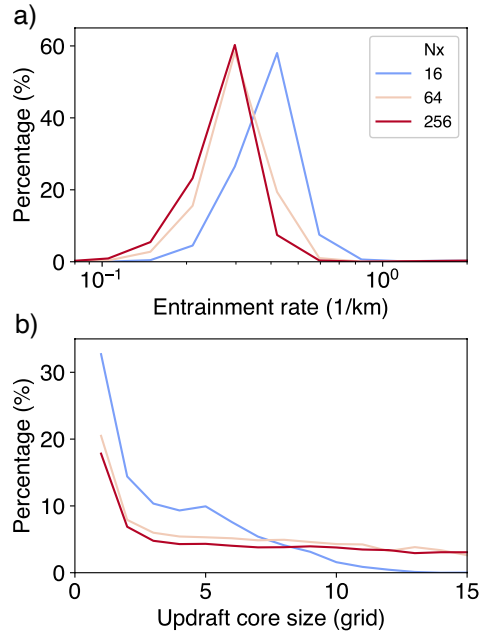


Figure 3. Probability distributions of (a) entrainment rate and (b) updraft width at 8 km. The entrainment rate distribution is diagnosed using the spectrum plume model described in Section 2.2. The core size distribution is calculated as the mass-flux-weighted number of updraft grid cells in each contiguous updraft core. A single core is determined as adjacent grid cells with upward velocity greater than 1 m s^{-1} and cloud mixing ratio greater than $10^{-5} \text{ kg kg}^{-1}$.

318 increases as computational domain sizes decreases. This is expected behavior even for
319 undilute convection.

320 Entrainment enhances this behavior. Updraft buoyancy reduction due to dilution
321 by entrainment is more likely as domain size decreases and updrafts become smaller. In
322 this way, enhanced entrainment also increases the impact of domain size on detrainment.
323 Figure 4q-t shows that as grid spacing decreases (and differences in entrainment between
324 computational domain sizes increases), the spread in detrainment rate with domain size
325 also increases, with the smallest domains at this highest resolution detraining the most.

326 **3.4 Domain size impacts on mean state variables and precipitation vari-** 327 **ability**

328 The mean relative humidity decreases with increasing computational and physi-
329 cal domain size (Figure 1c, Figure 4a-d). This is consistent with the sensitivity of en-
330 trainment and detrainment to domain size (see Romps, 2014), both of which increase
331 as domains (and their updrafts) become smaller. Unlike detrainment and entrainment,
332 which display narrowing distributions across computational domain sizes as grid spac-
333 ing is increased, the distribution of relative humidity does not narrow—it only shifts to-
334 wards lower values. Jeevanjee and Zhou (2022) discuss the sensitivity of relative humid-
335 ity to horizontal resolution.

336 A higher relative humidity in small domains implies that convection is less efficient
337 at heating the atmosphere due to enhanced evaporation. This explains why the convective
338 mass flux is larger for small domains (Figure 1a, Figure 4e-h). High cloud fractions
339 are also larger in small domains (Figure 1b). This is likely contributed to by the larger

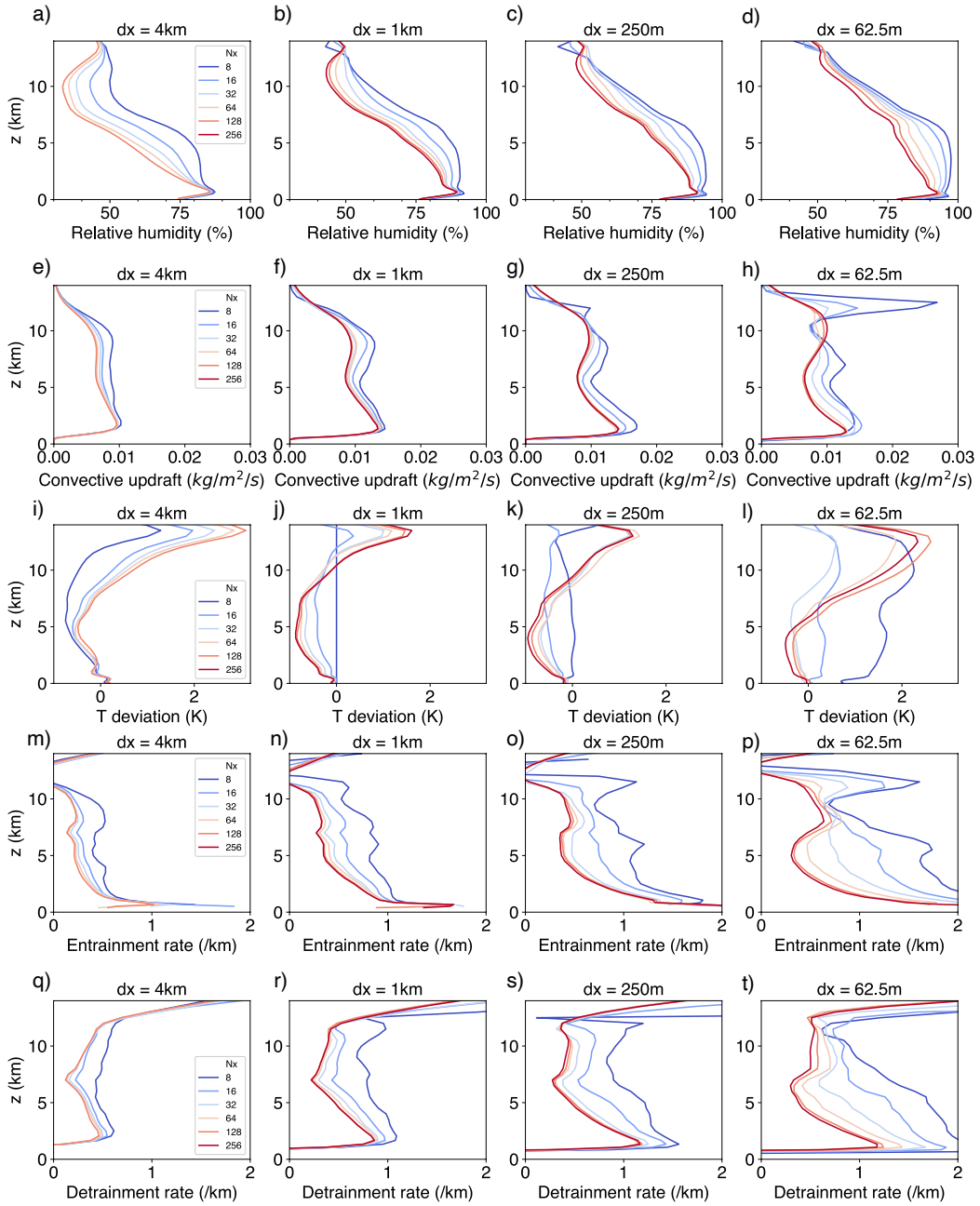


Figure 4. Sensitivity of domain mean profiles to computational domain size across horizontal resolutions of (left column), 1km (center left column), 250 m (center right column), and 62.5 m (right column). The rows from top-to-bottom are: (a-d) relative humidity, (e-h) updraft mass flux, (i-l) temperature deviation from $n_x=8$, (m-p) fractional entrainment rate, and (q-t) fractional detrainment rate. Entrainment and detrainment are diagnosed using the bulk plume model described in Section 2.2.

convective mass flux below the anvil level, which provides a larger anvil cloud source rate, as well as the higher relative humidity, which slows anvil cloud evaporation (Beydoun et al., 2021; Seeley et al., 2019). The change of temperature profiles may be viewed as mixture of two effects. On one hand, the stronger entrainment in the smaller domain tends to pull the temperature lapse rate away from moist pseudoadiabat lapse rate, making the temperature colder in smaller domain (Figure 4i). On the other, smaller domain also tends to have larger anvil cloud fraction and cloud radiative heating through the troposphere, which increases the temperature below anvil cloud in smaller domains (Figure 4j-l).

Figure 5 shows time series of precipitation, convective available potential energy (CAPE), and w_e . In addition to being higher, on average, the temporal variability of instability is also larger for small domains. The higher mean value of CAPE is a consequence of Equation (9): for small domains, the lapse rate needs to be larger (more unstable) to maintain a convective overturning circulation. In small domains, this manifests as periods of quiescence, when convection is suppressed, interspersed with periods of intense convection that occur when radiative cooling sufficiently steepens the lapse rate. In comparison, domain mean CAPE and precipitation are more consistent in time for large domains. This occurs, in part, because σ_c can be small in large domains, and consequently less instability is needed to maintain a convective circulation. The decreasing temporal variance with increasing computational domain size may also be contributed to by the increasing sample size.

4 Shallow convective cases

The heuristic argument of Section 3 hinges on the buoyancy condition that the rate of change of temperature in the convective region be larger than that of the subsiding non-convective region (Equation 6), and the implicit assumption that this condition must be satisfied in order for motion in the convective region to be ascending. While this is reasonable for deep convection, this may not capture the behavior of shallow convection as closely. For example, the boundary layer eddies that help maintain marine stratocumulus clouds are largely driven by strong radiative cooling at their tops (reviewed in Wood, 2012). Thus for completeness, we also tested the sensitivity of two shallow convective cases to computational domain size, described in Section 2.1. We used the BOMEX case to simulate trade cumulus, and we used the DYCOMS-RF01 case to simulate stratocumulus.

Figure 6 shows the 6-hour time series of cloud properties in the shallow convective simulations. Temporal variability for the small domains is much larger, likely due to the simulation only capturing the evolution of one or a small number of convective updrafts at a time. To enhance the signal-to-noise ratio of our results, we ran ensembles described in Section 2.1. The solid lines in Figure 6 represent the ensemble mean, while the shading represents the ensemble spread between the 25th to 75th quantiles. For both the BOMEX and DYCOMS-RF01 cases, the time evolution of cloud fraction and cloud water path converges for domains with at least 32×32 columns.

For the BOMEX case (Figure 6 left column), the smallest domain ($n_x=8$) shows significantly reduced cloud water path and slightly elevated cloud fraction compared to larger domains. These differences can also be viewed in the vertical profiles averaged over the last 2 hours (Figure 7). The updraft mass flux in $n_x=8$ has a very similar maximum value around 750 m but is shallower than the larger domains (Figure 7a). The faster decline of the updraft mass flux above the maximum indicates stronger detrainment (Figure 7d). This, taken together with the stronger diagnosed entrainment in $n_x=8$ (Figure 7c) is consistent with our result of stronger mixing for small domains from the deep convective simulations.

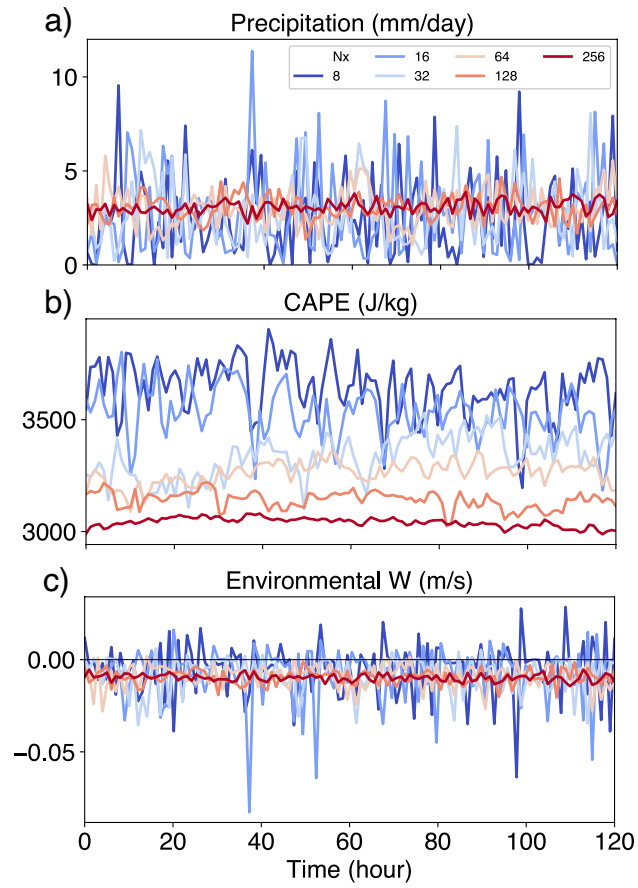


Figure 5. Time series of (a) surface precipitation, (b) convective available potential energy (CAPE), and (c) environmental vertical velocity across 5 days.

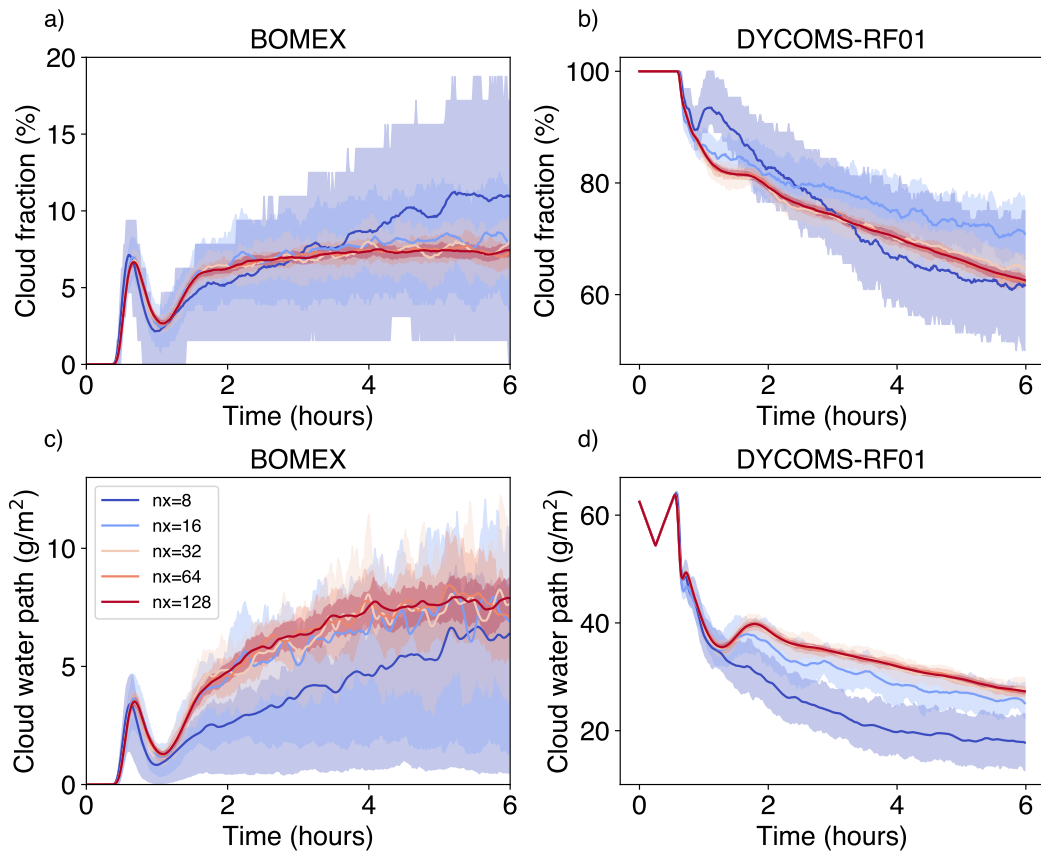


Figure 6. Time series of vertically integrated cloud fraction (top row) and cloud water path (bottom row) for the BOMEX case (left column) and the DYCOMS-RF01 case (right column). Solid lines are the ensemble mean, and the shading represents the 25th to 75th percentile of the ensemble spread. Cloud fraction here is defined as fraction of columns that have a cloud water path larger than 10 g m^{-2} .

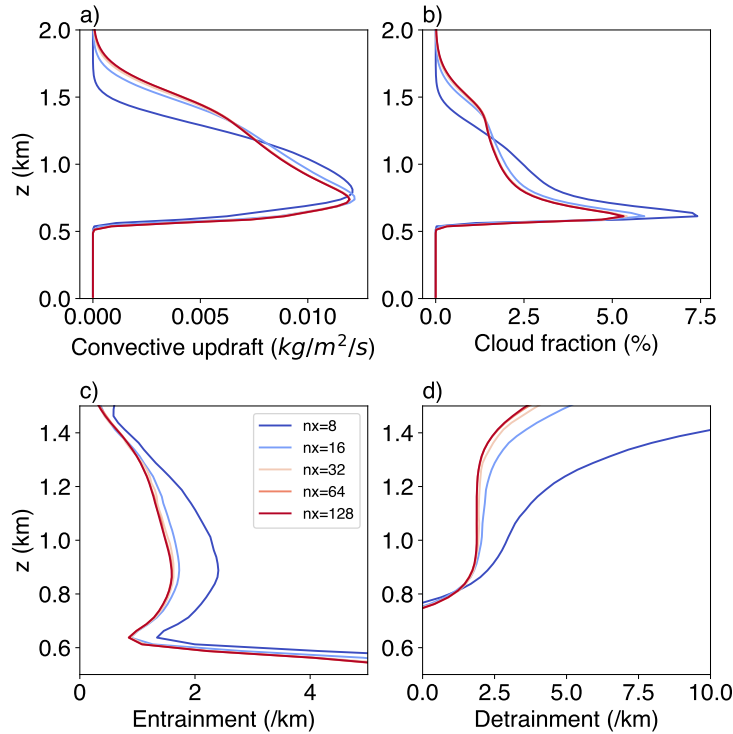


Figure 7. Mean atmosphere profiles over the last 2 hours in the BOMEX simulations: (a) updraft mass flux, (b) cloud fraction, (c) the fractional entrainment rate, and (d) the fractional detrainment rate. Entrainment and detrainment are diagnosed using the bulk plume model described in Section 2.2.

390 For the DYCOMS-RF01 stratocumulus case (Figure 6 right column), there is a sig-
 391 nificant reduction in the cloud water path for the two smaller domain sizes. For $nx=8$
 392 and $nx=16$, some ensemble members are able to sustain a larger cloud fraction than the
 393 larger domains. In $nx=8$, the stratocumulus cloud decks fully dissipate for some ensemble
 394 members (not shown). This may suggest that our smallest domain with 8×8 columns
 395 ($1\text{km} \times 1\text{km}$) is too small to sufficiently simulate stratocumulus and may trigger an in-
 396 stability that is sensitive to the initial noise perturbation. We encourage future studies
 397 to further explore this instability.

398 5 Summary

399 In simulations using convection resolving models (CRMs), small domains are used
 400 in both standalone simulations and within GCMs employing superparameterization or
 401 a multi-scale modeling framework. A CRM domain can be computationally small by hav-
 402 ing few grid columns, and it can also be physically small by representing a small phys-
 403 ical area.

404 Convective fractional area must be small in order to maintain positive buoyancy
 405 against a subsiding and warming environment. Small convective fractional area ensures
 406 that the downward mass flux is spread over a large area and hence, heats the environ-
 407 ment slowly. This is the same argument used to explain the observed smallness of the
 408 tropical convective ascent area (Bjerknes, 1938). In CRM domains, the smallest possi-
 409 ble convective fractional ascent area increases as the number of total grid columns de-
 410 creases. Consequently, convective fractional ascent area is forced to be large in CRM do-

411 mains with few grid columns and subsidence warming is strong, which suppresses con-
 412 vection. This argument is presented qualitatively in Pritchard et al. (2014).

413 Here, we present a heuristic argument to show why convection is “throttled”, or
 414 suppressed, in small domains. We show that

- 415 1. Small computational domains require more instability to sustain convection due
 416 to large convective fractional areas.
- 417 2. Physical updraft width is limited in both computationally and physically small
 418 domains, which increases updraft dilution by entrainment. This impact can be re-
 419 duced by increasing the grid spacing and by increasing the number of columns.
- 420 3. Detrainment occurs lower in the atmosphere for undilute convection in small do-
 421 mains. This is enhanced by the impact of domain size on updraft width and sub-
 422 sequent entrainment dilution.

423 As a result of “throttled” convection, the domain mean instability increases for small do-
 424 mains, and precipitation becomes more temporally variable, with periods of intense rain
 425 followed by relatively quiescent periods. Enhanced entrainment and detrainment in small
 426 domains increases the mean relative humidity, convective mass flux, and anvil cloud frac-
 427 tion. These conclusions are supported with CRM simulations of radiative convective equi-
 428 librium.

429 We also present results from shallow convective simulations across a range of do-
 430 main sizes for a shallow cumulus case and a marine stratocumulus case. In both cases,
 431 we see convergence of cloud properties when we increase the domain size. Similar to the
 432 deep convection simulations, the shallow cumulus simulations also show stronger en-
 433 trainment and detrainment rate in the small domains, leading to shallower updraft mass
 434 flux and cloud fraction. For the stratocumulus case, small domain seems to be more un-
 435 stable for cloud deck to maintain. This may suggest that it is insufficient to capture all
 436 the relevant processes for stratocumulus dynamics in a very small domain.

437 6 Discussion

438 An important new finding here is the suppression of convection that results from
 439 the limitation of updraft width by small domains, and subsequent strong entrainment
 440 dilution. This helps explain why simulated mean fields can still differ across larger do-
 441 mains, despite the expectation of convergent behavior beyond 32 columns for undiluted
 442 convection. We expect entrainment rates, and subsequent domain size sensitivity, to roughly
 443 converge at the domain size where the physical updraft width distribution is insensitive
 444 to domain size. In SAM, this occurs for domains with around 128×128 columns. Because
 445 this number is smaller for coarse grid spacing, we recommend using low horizontal res-
 446 olution for small computational domains simulating deep convection to avoid suppres-
 447 sion of deep convection. Additionally, the suggested domain sizes exhibiting convergence
 448 depend on entrainment and may be model dependent, as entrainment mixing relies, in
 449 part, on sub-grid schemes. Therefore, while all CRMs should show sensitivity to domain
 450 size, the precise size where convergence occurs could vary by model.

451 This study has direct implications for superparameterized modeling, which con-
 452 tinues to use computationally small domains because of the demanding computational
 453 cost. Pritchard et al. (2014) evaluate the climate of SP-GCM simulations with 8, 16, and
 454 32 columns in the embedded CRMs. A key result of their study was a stronger tropi-
 455 cal shortwave cloud forcing, which resulted from enhanced low-level liquid cloud and a
 456 drier and less cloudy upper troposphere. Also, the simulations with the smallest CRM
 457 domain produced more low intensity precipitation and less high intensity precipitation.
 458 These results differ from our results here. Our smallest domain simulations exhibit higher
 459 humidities throughout the troposphere, higher anvil cloud fractions, and a wider precip-

460 itation distribution. We hypothesize that these differences can be explained by circula-
 461 tions on the GCM grid that move energy between CRM domains in the SP setup. In an
 462 SP-GCM, convection can be continually suppressed in convectively stable regions because
 463 the CRM domain is not in energy balance. Conversely, in our simulations, the absence
 464 of a large-scale circulation means that convection has to happen somewhere in the do-
 465 main to balance radiative cooling.

466 The convective area fraction’s tight control by the domain lapse rate is in part a
 467 result of domain mass conservation ($\bar{w} = 0$). We can write the condition for convec-
 468 tion (6) because it is always true that environmental air is descending if there is convec-
 469 tion occurring. Consider however the case where $\bar{w} \neq 0$, for example in an SP-GCM where
 470 the CRM directly experiences the large-scale vertical motion of a host grid cell. Assum-
 471 ing condition (6) holds, (7) becomes

$$472 \quad \sigma_c < \frac{\Gamma_c - \Gamma_m - \frac{\bar{w}}{w_c}}{\Gamma_d - \Gamma_m + \Gamma_c - \Gamma_e}. \quad (12)$$

473 If $\bar{w} < 0$, condition (6) is still valid. However, convection may be less “throttled” be-
 474 cause the descending mean mass flux enables a larger maximum σ_c . That is, for a given
 475 computational domain size, convection may be triggered for less unstable profiles than
 476 is possible when \bar{w} *must* be zero. For large-scale ascent ($\bar{w} > 0$), environmental air is
 477 no longer guaranteed to be sinking and warming, and we can not claim (12) because of
 478 the potential for violation of condition (6). Currently, in both E3SM-MMF and SP-CESM,
 479 any large-scale vertical motion occurring on the GCM grid is communicated to the em-
 480 bedded CRM via a horizontally uniform forcing on the temperature (and moisture) ten-
 481 dencies (Grabowski, 2001), rather than on the velocity field. This does not impact the
 482 limitation of convective fractional ascent by the local lapse rate written in Equation (7).
 483 It remains to be seen if convective throttling is reduced in superparameterized simula-
 484 tions without strict enforcement of $\bar{w} = 0$.

485 Lastly, while quantitative, the argument we use to explain why a small CRM do-
 486 main “throttles” convection relies on a minimalist depiction of relations between vari-
 487 ables during convective motions. For example, radiation, which is not considered in our
 488 equations, may help reduce the critical lapse rate (Γ^*) needed to sustain an overturn-
 489 ing circulation for a given computational domain size because it heats the convective re-
 490 gion relative to the non-convective region and thus helps maintain condition (6). Sim-
 491 ilarly, we do not consider cooling in the environmental region due to evaporation of de-
 492 trained condensate, which may further help to reduce Γ^* . It is possible that these pro-
 493 cesses may have stronger effects than we anticipate. While entrainment is considered in
 494 a mostly qualitative sense in our discussion of the limitation of updraft width by domain
 495 size, we show in Figure 2 that it can have a large impact on Γ^* . Nonetheless, we believe
 496 that the model captures the primary relationships between variables that help explain
 497 convective throttling in small domains.

498 7 Data and Software Availability

499 Convection resolving model simulations were conducted with the System for At-
 500 mospheric Modeling (SAM) version 6.10.6 (M. Khairoutdinov, 2022).

501 Acknowledgments

502 This research has been supported by the National Oceanic and Atmospheric Adminis-
 503 tration Climate & Global Change Postdoctoral Fellowship Program through UCAR CPAESS
 504 Grant no. NA18NWS4620043B. This work used Bridges-2 at Pittsburgh Supercomput-
 505 ing Center through allocation EES230034 from the Advanced Cyberinfrastructure Co-
 506 ordination Ecosystem: Services & Support (ACCESS, Boerner et al., 2023) program, which
 507 is supported by National Science Foundation grants 2138259, 2138286, 2138307, 2137603,

508 and 2138296. We thank Zhiming Kuang, Kerry Emanuel, Xueying Yu, and Roger Samel-
509 son for helpful comments.

510 References

- 511 Beydoun, H., Caldwell, P. M., Hannah, W. M., & Donahue, A. S. (2021, August).
512 Dissecting anvil cloud response to sea surface warming. *Geophys. Res. Lett.*,
513 *48*(15).
- 514 Bjerknes, J. (1938). Saturated-adiabatic ascent of air through dry-adiabatically de-
515 scending environment. *Quart. J. Roy. Meteor. Soc.*, *64*, 325–330.
- 516 Boerner, T. J., Deems, S., Furlani, T. R., Knuth, S. L., & Towns, J. (2023, Septem-
517 ber). ACCESS: Advancing innovation: NSF’s advanced cyberinfrastructure
518 coordination ecosystem: Services & support. In *Practice and experience in
519 advanced research computing* (pp. 173–176). New York, NY, USA: Association
520 for Computing Machinery.
- 521 Grabowski, W. W. (2001, May). Coupling cloud processes with the Large-Scale dy-
522 namics using the Cloud-Resolving convection parameterization (CRCP). *J. At-
523 mos. Sci.*, *58*(9), 978–997.
- 524 Hannah, W. M., Jones, C. R., Hillman, B. R., Norman, M. R., Bader, D. C., Tay-
525 lor, M. A., . . . Lee, J. M. (2020, January). Initial results from the super-
526 parameterized E3SM. *J. Adv. Model. Earth Syst.*, *12*(1).
- 527 Hannah, W. M., Pressel, K., Ovchinnikov, M., & Elsaesser, G. (2022). Checker-
528 board patterns in E3SMv2 and E3SM-MMFv2. *Geoscientific Model Develop-
529 ment*, *15*(15), 6243–6257.
- 530 Holland, J. Z., & Rasmusson, E. M. (1973, January). Measurements of the atmo-
531 spheric mass, energy, and momentum budgets over a 500-kilometer square of
532 tropical ocean. *Mon. Weather Rev.*, *101*(1), 44–55.
- 533 Jeevanjee, N., & Zhou, L. (2022, March). On the resolution-dependence of anvil
534 cloud fraction and precipitation efficiency in radiative-convective equilibrium.
535 *J. Adv. Model. Earth Syst.*, *14*(3).
- 536 Khairoutdinov, M. (2022). *System for Atmospheric Modeling (version 6.10.6) [Soft-
537 ware]*. <http://rossby.msrc.sunysb.edu/~marat/SAM/>.
- 538 Khairoutdinov, M. F., & Randall, D. A. (2001, September). A cloud resolving model
539 as a cloud parameterization in the NCAR community climate system model:
540 Preliminary results. *Geophys. Res. Lett.*, *28*(18), 3617–3620.
- 541 Khairoutdinov, M. F., & Randall, D. A. (2003, February). Cloud resolving modeling
542 of the ARM summer 1997 IOP: Model formulation, results, uncertainties, and
543 sensitivities. *J. Atmos. Sci.*, *60*(4), 607–625.
- 544 Kuang, Z., & Bretherton, C. S. (2006). A mass-flux scheme view of a high-resolution
545 simulation of a transition from shallow to deep cumulus convection. *Journal of
546 the Atmospheric Sciences*, *63*(7), 1895–1909.
- 547 Lin, G., Jones, C. R., Leung, L. R., Feng, Z., & Ovchinnikov, M. (2022, January).
548 Mesoscale convective systems in a superparameterized E3SM simulation at
549 high resolution. *J. Adv. Model. Earth Syst.*, *14*(1).
- 550 Liu, N., Pritchard, M. S., Jenney, A. M., & Hannah, W. M. (2023, April). Un-
551 derstanding precipitation bias sensitivities in E3SM-multi-scale modeling
552 framework from a dilution framework. *J. Adv. Model. Earth Syst.*, *15*(4).
- 553 Morrison, H. (2017, March). An analytic description of the structure and evolution
554 of growing deep cumulus updrafts. *J. Atmos. Sci.*, *74*(3), 809–834.
- 555 Morrison, H., Peters, J. M., Varble, A. C., Hannah, W. M., & Giangrande, S. E.
556 (2020, October). Thermal chains and entrainment in cumulus updrafts. part i:
557 Theoretical description. *J. Atmos. Sci.*, *77*(11), 3637–3660.
- 558 Muller, C. J., & Held, I. M. (2012, August). Detailed investigation of the Self-
559 Aggregation of convection in Cloud-Resolving simulations. *J. Atmos. Sci.*,
560 *69*(8), 2551–2565.

- 561 Patrizio, C. R., & Randall, D. A. (2019, July). Sensitivity of convective self-
562 aggregation to domain size. *J. Adv. Model. Earth Syst.*, *11*(7), 1995–2019.
- 563 Peng, L., Pritchard, M., Blossey, P. N., Hannah, W. M., Bretherton, C. S., Terai,
564 C. R., & Jenney, A. M. (2023). Improving stratocumulus cloud amounts in a
565 200-m resolution multi-scale modeling framework through tuning of its interior
566 physics. *ESS Open Archive*.
- 567 Peng, L., Pritchard, M., Hannah, W. M., Blossey, P. N., Worley, P. H., & Brether-
568 ton, C. S. (2022, May). Load-balancing intense physics calculations to embed
569 regionalized high-resolution cloud resolving models in the E3SM and CESM
570 climate models. *J. Adv. Model. Earth Syst.*, *14*(5).
- 571 Pritchard, M. S., Bretherton, C. S., & DeMott, C. A. (2014, September). Restricting
572 32-128 km horizontal scales hardly affects the MJO in the superparameterized
573 community atmosphere model v.3.0 but the number of cloud-resolving grid
574 columns constrains vertical mixing. *J. Adv. Model. Earth Syst.*, *6*(3), 723–739.
- 575 Romps, D. M. (2014, October). An analytical model for tropical relative humidity.
576 *J. Clim.*, *27*(19), 7432–7449.
- 577 Seeley, J. T., Jeevanjee, N., Langhans, W., & Romps, D. M. (2019, January). For-
578 mation of tropical anvil clouds by slow evaporation. *Geophys. Res. Lett.*,
579 *46*(1), 492–501.
- 580 Siebesma, A. P., Bretherton, C. S., Brown, A., Chlond, A., Cuxart, J., Duynkerke,
581 P. G., ... Others (2003). A large eddy simulation intercomparison study of
582 shallow cumulus convection. *J. Atmos. Sci.*, *60*(10), 1201–1219.
- 583 Stevens, B., Moeng, C.-H., Ackerman, A. S., Bretherton, C. S., Chlond, A., de
584 Roode, S., ... others (2005). Evaluation of large-eddy simulations via obser-
585 vations of nocturnal marine stratocumulus. *Monthly weather review*, *133*(6),
586 1443–1462.
- 587 Wing, A. A., Reed, K. A., Satoh, M., Stevens, B., Bony, S., & Ohno, T. (2018,
588 March). Radiative–convective equilibrium model intercomparison project.
589 *Geoscientific Model Development*, *11*(2), 793–813.
- 590 Wing, A. A., Stauffer, C. L., Becker, T., Reed, K. A., Ahn, M., Arnold, N. P., ...
591 Zhao, M. (2020, July). Clouds and convective Self-Aggregation in a Multi-
592 Model ensemble of Radiative-Convective equilibrium simulations. *J. Adv.*
593 *Model. Earth Syst.*
- 594 Wood, R. (2012, August). Stratocumulus clouds. *Mon. Weather Rev.*, *140*(8), 2373–
595 2423.
- 596 Yanase, T., Nishizawa, S., Miura, H., Takemi, T., & Tomita, H. (2020, August).
597 New critical length for the onset of self-aggregation of moist convection. *Geo-*
598 *phys. Res. Lett.*, *47*(16).